First Examples of Thallium Chalcogenide Cages. Syntheses, ^{77}Se, ^{203}Tl, and ^{205}Tl NMR Study of the $Tl_4Se_5^{4-}$ and $Tl_4Se_6^{4-}$ Anions, the X-ray Crystal Structure of $(2,2,2\text{-crypt-}K^+)_3Tl_5Se_5^{3-}$, and Theoretical Studies†

Janette Campbell,‡ Hélène P. A. Mercier,*,‡ David P. Santry,§ Reijo J. Suontamo,|| Horst Borrmann,⊥ and Gary J. Schrobilgen*,‡

Department of Chemistry, McMaster University, Hamilton, Ontario L8S 4M1, Canada; Snowbird Software, Inc., 71A Leland Street, Hamilton, Ontario, L8S 3A1, Canada; Department of Chemistry, University of Jyväskylä, P.O. Box 35, FIN-40351 Jyväskylä, Finland; and Max-Planck-Institut für Chemische Physik fester Stoffe, Raum B1.2.11, Nöthnitzer Strasse 40, Dresden D-01187, Germany

Received July 14, 2000

The $Tl_5Se_5^{3-}$ anion has been obtained by extracting KTlSe in ethylenediamine in the presence of 2,2,2-crypt. The salt, $(2,2,2\text{-crypt-}K^+)_3Tl_5Se_5^{3-}$, crystallizes in the triclinic system, space group $P\bar{1}$, with $Z = 2$ and $a = 11.676(2)$ Å, $b = 16.017(3)$ Å, $c = 25.421(5)$ Å, $\alpha = 82.42(3)°$, $\beta = 88.47(3)°$, $\gamma = 69.03(3)°$ at −123 °C. Two other mixed oxidation state Tl^I/Tl^{III} anions, $Tl_4Se_5^{4-}$ and $Tl_4Se_6^{4-}$, have been obtained by extracting KTlSe into liquid NH_3 in the presence of 2,2,2-crypt and have been characterized in solution by low-temperature ^{77}Se, ^{203}Tl, and ^{205}Tl NMR spectroscopy and were shown to exist as a 1:1 equilibrium mixture at −40 °C. The couplings, $^1J(^{203,205}Tl-^{77}Se)$ and $^2J(^{203,205}Tl-^{203,205}Tl)$, have been observed for $Tl_4Se_5^{4-}$ and $Tl_4Se_6^{4-}$ and have been used to arrive at the solution structures of both anions. Structural assignments were achieved by detailed analyses and simulations of all spin multiplets that comprise the ^{205,203}Tl NMR spectra and that arise from natural abundance ^{205,203}Tl and ^{77}Se or enriched ^{77}Se isotopomer distributions. The structures of all three anions are based on a Tl_4Se_4 cube in which Tl and Se atoms occupy alternate corners. There are one and two exo-selenium atoms bonded to thallium in $Tl_4Se_5^{4-}$ and $Tl_4Se_6^{4-}$, respectively, so that these thalliums are four-coordinate and possess a formal oxidation state of +3 and the remaining three-coordinate thallium atoms are in the +1 oxidation state. The structure of $Tl_5Se_5^{3-}$ may be formally regarded as an adduct in which Tl^+ is coordinated to the unique exo-selenium and to two seleniums in a cube face containing the Tl^{III} atom. The $Tl_4Se_5^{4-}$, $Tl_4Se_6^{4-}$, and $Tl_5Se_5^{3-}$ anions and the presently unknown, but structurally related, $Tl_4Se_4^{4-}$ anion can be described as electron-precise cages. Ab initio methods at the MP2 level of theory show that $Tl_4Se_5^{4-}$, $Tl_4Se_6^{4-}$, and $Tl_5Se_5^{3-}$ exhibit true minima and display geometrical parameters that are in excellent agreement with their experimental cubanoid structures, and that $Tl_4Se_4^{4-}$ is cube-shaped (T_d point symmetry). The gas-phase energetics associated with plausible routes to the formation and interconversions of these anions have been determined by ab initio methods and assessed. It is proposed that all three cubanoid anions are derived from the known $Tl_2Se_2^{2-}$, $TlSe_3^{3-}$, Se_2^{2-}, and polyselenide anions that have been shown to be present in the solutions they are derived from.

Introduction

Few thallium chalcogenide anions have been fully characterized in the solid state or in solution. Those that have been studied by X-ray crystallography include the $Tl_2Ch_2^{2-}$ (Ch = Se, Te),[1,2] $Tl_3Se_3(Se_4)_3^{3-}$,[3] $Tl_4Se_{16}^{4-}$,[4] and the $[Tl(Se_6)_2]_n^{n-}$ [5] anions. With the exception of the $Tl_2Ch_2^{2-}$ anions, which adopt butterfly geometries and contain Tl^I atoms, all other anions contain thallium in the +3 oxidation state, and none are cages. The Tl^{III} atoms of the $Tl_3Se_3(Se_4)_3^{3-}$ anion form a ring in which the thallium atoms are bridged by monoselenides and each Tl atom of the Tl_3Se_3 ring is coordinated to a bidentate Se_4 group, completing its tetrahedral coordination. The $Tl_4Se_{16}^{4-}$ anion is a chain structure featuring four linearly arranged tetrahedral Tl^{III} atoms in which each terminal Tl atom is coordinated to a bidentate Se_4 group and an Se ligand that bridge to each of the two central Tl atoms. The two central Tl atoms are, in turn, linked by two bridging Se atoms to give a central Tl_2Se_2 ring. The $[Tl(Se_6)_2]_n^{n-}$ structure consists of tetrahedral Tl^{III} centers and bridging Se_6 ligands, leading to a two-dimensional extended structure. The only mixed oxidation state thallium selenide is TlSe, or $Tl^I(Tl^{III}Se_2)$.[6,7] The structure comprises chains made up of Tl^{III} atoms tetrahedrally coordinated to Se atoms that are, in turn, bridged to Tl^I atoms to give an extended structure.

† Dedicated to the memory of Professor Olivier Kahn (September 13, 1942 to December 8, 1999), who was a dedicated and outstanding researcher and teacher who transmitted to others his enthusiasm for research.

* To whom correspondence should be sent.
‡ McMaster University.
§ Snowbird Software, Inc.
|| University of Jyväskylä.
⊥ Max-Planck-Institut.

(1) Burns, R. C.; Corbett, J. D. *J. Am. Chem. Soc.* **1981**, *103*, 2627.
(2) Borrmann, H.; Campbell, J.; Dixon, D. A.; Mercier, H. P. A.; Pirani, A. M.; Schrobilgen, G. J. *Inorg. Chem.* **1998**, *37*, 1929.
(3) Dhingra, S.; Kanatzidis, M. *Inorg. Chem.* **1993**, *32*, 1350.
(4) Dhingra, S.; Liu, F.; Kanatzidis, M. G. *Inorg. Chim. Acta* **1993**, *210*, 237.
(5) Dhingra, S.; Kanatzidis, M. G. *Science* **1992**, *258*, 1769.
(6) Ketelaar, J. A. A.; t'Hart, W. H.; Moerel, M.; Polder, D. *Z. Kristallogr.* **1939**, *A101*, 396.
(7) Man, L. I.; Imamov, R. M.; Semiletov, S. A. *Kristallografiya* **1976**, *21*, 628; *Sov. Phys. Crystallogr.* **1976**, *21*, 355.

10.1021/ic000779d CCC: $20.00
Published on Web 12/14/2000

The trigonal planar $Tl^{I}Ch_3^{3-}$ [8] and the butterfly-shaped $Tl^{III}_2Ch_2^{2-}$ [2,8] anions are the only thallium chalcogenide polyanions that have been fully characterized in solution by $^{203,205}Tl$, ^{77}Se, and ^{125}Te NMR spectroscopy. Although the $Tl^{III}_3Se_3(Se_4)_3^{3-}$ anion has been characterized by variable-temperature ^{77}Se NMR spectroscopy, neither $^1J(^{205,203}Tl-^{77}Se)$ nor $^1J(^{77}Se-^{77}Se)$ couplings were observed.[3] Solution multi-NMR studies have proven to be very successful in corroborating the solution structures of many anions otherwise characterized in the solid state and for the structural characterization of main group chalcogenide anions, which could only be characterized in solution and which do not provide crystalline material suitable for single-crystal X-ray structure determinations.[2,9−17] Although the use of thallium NMR spectroscopy is not prevalent because the Larmor frequencies of ^{203}Tl and ^{205}Tl lie outside the ranges of commercial broadband multi-NMR probes, the large differences in chemical shift associated with the +1 and +3 oxidation states of thallium have proven to be useful in establishing the formal oxidation state of thallium in chalcogenide anions.[2,8]

The present paper reports the detailed variable-temperature solution multi-NMR spectroscopic characterization of two new mixed Tl^{I}/Tl^{III} anions, the $Tl_4Se_5^{4-}$ and $Tl_4Se_6^{4-}$ anions, and the X-ray crystal structure of a third novel mixed thallium oxidation state anion, $Tl_5Se_5^{3-}$. The three anion structures are based on cubic arrangements of Tl and Se atoms and represent the first examples of thallium chalcogenide cages. Preliminary evidence is also given for the existence of a mixed oxidation state trithallium selenide anion.

Results and Discussion

Synthesis of the Tetrathallium Selenide Anions. The synthetic approach was essentially that reported earlier[8] and consisted of the extraction of KTlSe powder and 94.4% ^{77}Se-enriched KTlSe (hereafter referred to as KTl^{77}Se) in liquid NH_3 or ethylenediamine (en) in the presence of an excess of 2,2,2-crypt (4,7,13,16,21,24-hexaoxa-1,10-diazabicyclo[8.8.8]hexacosane) with respect to K^+. The earlier multi-NMR study[8] noted the presence of other Tl/Se species in addition to the $TlSe_3^{3-}$, $Tl_2Se_2^{2-}$, and Se^{2-} anions. Several of these species have been identified in the present study by $^{203,205}Tl$ and ^{77}Se NMR spectroscopy as the $Tl_4Se_5^{4-}$ and $Tl_4Se_6^{4-}$ anions (see Solution Characterization of the $Tl_4Se_5^{4-}$ and $Tl_4Se_6^{4-}$ Anions by NMR Spectroscopy). The en extract of KTlSe was also shown by $^{203,205}Tl$ NMR spectroscopy to contain a trithallium anion $Tl_3Se_x^{y-}$, which has also been observed in liquid NH_3 extracts of $NaTl_{0.5}Se$ and in en and liquid NH_3 extracts of NaTlSe.[18]

Table 1. Summary of Crystal Data and Refinement Results for $(2,2,2\text{-crypt-}K^+)_3Tl_5Se_5^{3-}$

formula	$C_{54}H_{108}K_5N_6O_{18}Se_5Tl_5$
fw	2663.42
space group (No.)	$P\bar{1}$ (2)
a (Å)	11.818(2)
b (Å)	16.118(3)
c (Å)	25.765(5)
α (deg)	82.56(3)
β (deg)	88.62(3)
γ (deg)	68.95(3)
V (Å^3)	4540(2)
Z	2
temp (°C)	−123
λ (Å)	0.710 73
ρ_{calcd} (g cm^{-3})	1.948
μ (cm^{-1})	110.4
R_1[a]	0.1418
wR_2[b]	0.3447

[a] $R_1 = \sum||F_o| - |F_c||/\sum|F_o|$ for $I > 2\sigma(I)$. [b] $wR_2 = [\sum[w(F_o^2 - F_c^2)^2]/\sum w(F_o^2)^2]^{1/2}$ for $I > 2\sigma(I)$.

In the course of this study, crystals of the known $(2,2,2\text{-crypt-}K^+)_2Se_5^{2-}$ salt[19] were obtained from an en solution of KTlSe containing a molar excess of 2,2,2-crypt with respect to K^+. Upon addition of THF to an identical solution, crystals of $(2,2,2\text{-crypt-}K^+)_2Tl_2Se_2^{2-}$ were obtained. Thin, red platelets of $(2,2,2\text{-crypt-}K^+)_3Tl_5Se_5^{3-}$ were obtained upon addition of THF to dimethylformamide (DMF) extracts of KTlSe in the presence of 2,2,2-crypt. When the crystalline material was briefly dried under dynamic vacuum (i.e., longer than 2 min), some degradation was observed. It can be assumed that this degradation was caused by significant loss of solvent from the crystal lattice.

X-ray Crystal Structure of $(2,2,2\text{-crypt-}K^+)_3Tl_5Se_5^{3-}$. A summary of the crystal data and refinement results is given in Table 1. The most significant bond lengths, bond angles, and long contact distances are given in Table 2. The crystal structure of $(2,2,2\text{-crypt-}K^+)_3Tl_5Se_5^{3-}$ consists of well-separated and ordered $Tl_5Se_5^{3-}$ anions (Figure 1) and 2,2,2-crypt-K^+ cations as well as unresolved solvent molecules filling large channels running parallel to the a axis (see Experimental Section and Figure 2).

The structure of the 2,2,2-crypt-K^+ cation is similar to those previously reported in $(2,2,2\text{-crypt-}K^+)_4Sn_4Se_{10}^{4-}$ [20] and $(2,2,2\text{-crypt-}K^+)_2Pb_2Ch_3^{2-}\cdot 0.5en$,[17] with average K···O and K···N distances of 2.66(2)−2.90(4) and 2.93(4)−3.10(4) Å and is not discussed further.

The $Tl_5Se_5^{3-}$ anion (Figure 1) consists of a distorted Tl_4Se_4 cube with one face capped by a fifth thallium atom [Tl(5)]. The Tl(5) atom is located in the diagonal plane of the cube [Tl(3), Tl(4), Se(1), Se(2)] containing the capping Se(5) atom and is bonded to the face of the cube through the two Tl(5)−Se(3,4) bonds and bridges to a third selenium, Se(5), which is also coordinated to the Tl^{III} atom, Tl(4). The cube framework of the $Tl_5Se_5^{3-}$ anion contains a unique and approximately tetrahedrally coordinated Tl^{III} atom [Tl(4)], four Tl^{I} atoms [Tl(1,2,3,5)] having trigonal pyramidal coordination, and bridging Se atoms that are dicoordinate [Se(5)], tricoordinate [Se(1,2)], and tetracoordinate [Se(3,4)].

The 4 Tl^{III}−Se distances (2.543(4)−2.766(3) Å) are significantly shorter than the 12 Tl^{I}−Se distances (2.814(4)−3.039(4) Å) in $Tl_5Se_5^{3-}$ and are similar to those for other tetracoordinate Tl^{III} selenide anions, i.e., $Tl_3Se_3(Se_4)_3^{3-}$ [2.585(5)−

(8) Burns, R. C.; Devereux, L. A.; Granger, P.; Schrobilgen, G. J. *Inorg. Chem.* **1985**, *24*, 2615.
(9) Campbell, J.; Devereux, L. A.; Gerken, M.; Mercier, H. P. A.; Pirani, A. M.; Schrobilgen, G. J. *Inorg. Chem.* **1996**, *35*, 2945.
(10) Rudolph, R. W.; Wilson, W. L.; Parker, F.; Taylor, R. C.; Young, D. C. *J. Am. Chem. Soc.* **1978**, *100*, 4629.
(11) Rudolph, R. W.; Taylor, R. C.; Young, D. C. In *Fundamental Research in Homogeneous Catalysis*; Tsutsui, M., Ed.; Plenum Press: New York, 1979; p 997.
(12) Pons, B. S.; Santure, D. J.; Taylor, R. C.; Rudolph, R. W. *Electrochem. Acta* **1981**, *26*, 365.
(13) Rudolph, R. W.; Wilson, W. L. *J. Am. Chem. Soc.* **1981**, *103*, 2480.
(14) Wilson, W. L.; Rudolph, R. W.; Lohr, L. L.; Taylor, R. C.; Pyykkö, P. *Inorg. Chem.* **1986**, *25*, 1535.
(15) Björgvinsson, M.; Sawyer, J. F.; Schrobilgen, G. J. *Inorg. Chem.* **1991**, *30*, 4238.
(16) Björgvinsson, M.; Mercier, H. P. A.; Mitchell, K. M.; Schrobilgen, G. J.; Strohe, G. *Inorg. Chem.* **1993**, *34*, 6046.
(17) Borrmann, H.; Campbell, J.; Dixon, D. A.; Mercier, H. P. A.; Pirani, A. M.; Schrobilgen, G. J. *Inorg. Chem.* **1998**, *37*, 6656.
(18) Pirani, A. M.; Mercier, H. P. A.; Santry, D. P.; Suontamo, R. J.; Borrmann, H.; Schrobilgen, G. J. *Inorg. Chem.*, to be submitted.
(19) Müller, V.; Ahle, A.; Frenzen, G.; Neumüller, B.; Dehnicke, K. *Z. Anorg. Allg. Chem.* **1993**, *619*, 1247.
(20) Campbell, J.; DiCiommo, D. P.; Mercier, H. P. A.; Pirani, A. M.; Schrobilgen, G. J.; Willuhn, M. *Inorg. Chem.* **1995**, *34*, 6265.

Table 2. Experimental and Calculated Geometries for the $Tl_5Se_5^{3-}$ Anion

Bond Lengths and Contacts (Å)

	exptl	MP2 (C_1)	MP2 (C_s)		exptl	MP2 (C_1)	MP2 (C_s)
Tl(1)−Se(1)	2.890(4)	2.980	2.979	Tl(1)−Se(2)	3.045(4)	3.227	3.227
Tl(1)−Se(4)	3.052(3)	3.183	3.183	Tl(2)−Se(1)	2.881(4)	2.980	2.979
Tl(2)−Se(2)	3.047(4)	3.227	3.227	Tl(2)−Se(3)	3.089(4)	3.183	3.183
Tl(3)−Se(1)	2.849(4)	3.037	3.037	Tl(3)−Se(3)	3.003(4)	3.116	3.117
Tl(3)−Se(4)	3.053(4)	3.116	3.117	Tl(4)−Se(2)	2.564(4)	2.637	2.637
Tl(4)−Se(3)	2.755(4)	2.826	2.825	Tl(4)−Se(4)	2.802(3)	2.824	2.825
Tl(4)−Se(5)	2.603(5)	2.660	2.660	Tl(5)−Se(3)	3.057(4)	3.175	3.178
Tl(5)−Se(4)	3.046(4)	3.179	3.178	Tl(5)−Se(5)	3.050(5)	3.047	3.047
Tl(1)···Tl(4)	3.778(2)	3.892	3.891	Tl(2)···Tl(4)	3.744(3)	3.891	3.891
Tl(3)···Tl(5)	3.637(3)	3.995	3.995	Tl(4)···Tl(5)	3.209(2)	3.361	3.361
Tl(1)···Tl(2)	4.007(2)	4.167	4.167	Tl(1)···Tl(3)	3.940(3)	4.103	4.102
Tl(2)···Tl(3)	3.940(2)	4.102	4.102	Tl(3)···Tl(4)	4.037(2)	4.257	4.257

Bond Angles (deg)

	exptl	MP2 (C_1)	MP2 (C_s)		exptl	MP2 (C_1)	MP2 (C_s)
Se(1)−Tl(1)−Se(2)	94.66(10)	95.1	95.1	Se(1)−Tl(1)−Se(4)	95.96(10)	96.1	96.1
Se(2)−Tl(1)−Se(4)	88.92(10)	87.6	87.6	Se(1)−Tl(2)−Se(2)	94.80(10)	95.1	95.1
Se(1)−Tl(2)−Se(3)	94.96(11)	96.1	96.1	Se(2)−Tl(2)−Se(3)	88.90(10)	87.6	87.6
Se(1)−Tl(3)−Se(3)	97.55(11)	96.4	96.4	Se(1)−Tl(3)−Se(4)	96.79(10)	96.4	96.4
Se(3)−Tl(3)−Se(4)	84.08(10)	79.9	79.9	Se(2)−Tl(4)−Se(3)	107.71(12)	108.6	108.6
Se(2)−Tl(4)−Se(4)	105.37(11)	108.6	108.6	Se(2)−Tl(4)−Se(5)	138.71(13)	136.9	136.9
Se(3)−Tl(4)−Se(4)	93.75(11)	90.2	90.2	Se(3)−Tl(4)−Se(5)	100.48(13)	101.3	101.4
Se(4)−Tl(4)−Se(5)	102.15(13)	101.4	101.4	Se(3)−Tl(5)−Se(4)	84.85(12)	78.0	78.1
Se(3)−Tl(5)−Se(5)	84.85(12)	86.0	86.0	Se(4)−Tl(5)−Se(5)	87.28((11)	86.0	86.0
Tl(1)−Se(1)−Tl(2)	87.98(10)	88.7	88.7	Tl(1)−Se(1)−Tl(3)	86.78(11)	85.9	86.0
Tl(2)−Se(1)−Tl(3)	86.87(11)	86.0	86.0	Tl(1)−Se(2)−Tl(2)	82.29(9)	80.4	80.4
Tl(1)−Se(2)−Tl(4)	84.21(11)	82.5	82.5	Tl(2)−Se(2)−Tl(4)	83.23(11)	82.5	82.5
Tl(2)−Se(3)−Tl(3)	80.57(10)	81.3	81.3	Tl(2)−Se(3)−Tl(4)	79.45(10)	80.5	80.5
Tl(2)−Se(3)−Tl(5)	137.43(14)	141.8	141.8	Tl(3)−Se(3)−Tl(4)	88.88(12)	91.4	91.4
Tl(3)−Se(3)−Tl(5)	73.83(10)	78.8	78.8	Tl(4)−Se(3)−Tl(5)	66.80(9)	67.8	67.8
Tl(1)−Se(4)−Tl(3)	80.43(9)	81.2	81.3	Tl(1)−Se(4)−Tl(4)	80.25(9)	80.5	80.5
Tl(1)−Se(4)−Tl(5)	137.98(12)	141.7	141.6	Tl(3)−Se(4)−Tl(4)	87.01(9)	91.4	91.4
Tl(3)−Se(4)−Tl(5)	73.28(9)	78.8	78.8	Tl(4)−Se(4)−Tl(5)	66.40(8)	67.8	67.8
Tl(4)−Se(5)−Tl(5)	68.65(11)	71.8	71.8				

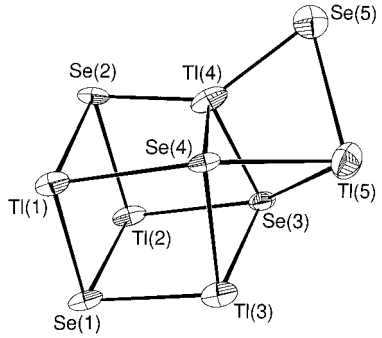

Figure 1. Crystal structure of the $Tl_5Se_5^{3-}$ anion in (2,2,2-crypt-K^+)$_3$-$Tl_5Se_5^{3-}$. Thermal ellipsoids are drawn at the 50% probability level.

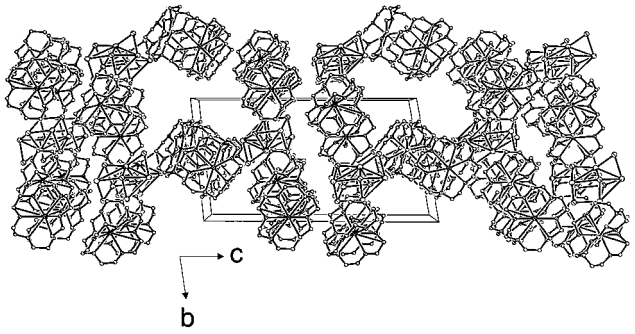

Figure 2. Unit cell of (2,2,2,-crypt-K^+)$_3$$Tl_5Se_5^{3-}$ viewed down the *a* axis.

2.686(6) Å],[3] $Tl_4Se_{16}^{4-}$ [2.584(7)−2.802(8) Å],[4] $[Tl(Se_6)_2]_n^{n-}$ [2.639(2) Å],[5] and $Tl^I(Tl^{III}Se_2)$ [2.68 Å].[6,7] The Tl(4)−Se(2,5) distances [2.543(4) and 2.579(4) Å] are shorter than those involving the tetracoordinated Se(3) and Se(4) atoms [2.766(3) and 2.729(4) Å, respectively].

The Tl^I−Se bond lengths within the [Tl(1,2), Se(1,2)] face can be divided into two ranges: Tl−Se(1) [2.849(4) and 2.890(4) Å] and Tl−Se(2) [3.045(4) and 3.047(4) Å]. The coordination of Se(2) to the Tl^{III} center, Tl(4), results in the elongation of the Tl(1,2)−Se(2) distances and in a smaller Tl(1)−Se(2)−Tl(2) [82.29(9)°] angle when compared with Tl(1)−Se(1)−Tl(2) [87.98(10)°]. The Tl(3)−Se distances consist of one short [Se(1), 2.849(4) Å] and two longer [Se(3), 3.003(4) Å; Se(4), 3.053(4) Å] bond lengths. The shorter distance involves Se(1), which is only bonded to Tl^I atoms, whereas Se(3) and Se(4) are also bonded to the Tl^{III} atom. The capping thallium (Tl(5)) is positioned above the center of the [Tl(3,4), Se(3,4)] face and has two contacts to selenium atoms in this face, namely, Tl(5)−Se(3), 3.057(4) Å, and Tl(5)−Se(4), 3.046(4) Å, and a contact to the exo-selenium Se(5), 3.050(5) Å. These distances are essentially equal and are significantly less than the sum of the Se^{2-} and Tl^+ ionic radii (1.50 + 1.98 = 3.48 Å).[21] The Tl^I−Se distances in $Tl_5Se_5^{3-}$ [2.849(4)−3.057(4) Å] are shorter than those in $Tl^I(Tl^{III}Se_2)$ [3.42 Å][6,7] and $Tl_2(Se_2C_2(CN)_2)_2^{2-}$ [3.132(2)−3.207(2) Å][22] but are longer than those in the $Tl_2Se_2^{2-}$ [2] anion [2.781(3) Å]. This variation can be explained by considering the coordination numbers of the Tl^I atoms. In the $Tl_2Se_2^{2-}$ anion, the Tl atoms are dicoordinate and, as expected, represent the shortest Tl−Se distances, whereas those

(21) Shannon, R. D. *Acta Crystallogr.* **1976**, *A32*, 751.
(22) Hummel, H.-U.; Fischer, E.; Fischer, T.; Gruss, D.; Franke, A.; Dietzsch, W. *Chem. Ber.* **1992**, *125*, 1565.

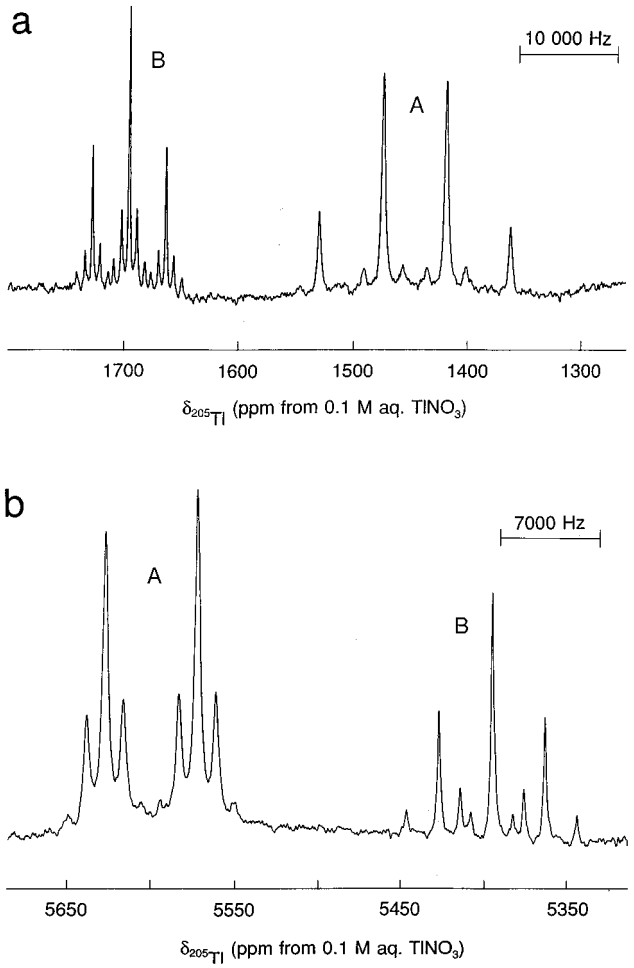

Figure 3. ^{205}Tl (115.444 MHz) NMR spectra of the (a) Tl(I) and (b) Tl(III) environments in (A) $Tl_4Se_5^{4-}$ and (B) $Tl_4Se_6^{4-}$ anions recorded in liquid NH_3 at −40 °C.

in $Tl^I(Tl^{III}Se_2)$ and $Tl_2(Se_2C_2(CN)_2)_2^{2-}$ exhibit octa- and tetracoordination, respectively, and the longest Tl^I−Se bond lengths. Intermediate values are observed for $Tl_5Se_5^{3-}$, which contains only tricoordinate Tl^I atoms. The variation in Tl^I−Se distances with Tl^I coordination number is consistent with the bond valence concept.[23,24]

The [Tl(1,2), Se(1,2)], [Tl(1,3), Se(1,4)], and [Tl(2,3), Se(1,3)] faces deviate little from planarity, i.e., 0.048, 0.019, and 0.021 Å, respectively, with their intrafacial Se−Tl−Se angles ranging from 86.78(12)° to 93.75(11)°. In contrast, the remaining faces that incorporate the Tl^{III} atom show larger deviations from planarity ([Tl(1,4), Se(2,4)], 0.102 Å; [Tl(2,4), Se(2,3)], 0.076 Å; [Tl(3,4), Se(3,4)], 0.236 Å). The distortions are mainly a consequence of the tetrahedral coordination of Tl^{III}, which displays intrafacial Se−Tl(4)−Se angles [105.4(1)−107.7(1)°] that are only somewhat compressed with respect to the ideal tetrahedral angle. The angle formed by the Tl(4)−Se(5) bond exo to the Tl_4Se_4 cube and the only tricoordinate cage selenium, Se(2), adjacent to Tl(4) is correspondingly more open (158.9(2)°) than the remaining Se−Tl−Se intrafacial angles. The Se(3)−Tl(4)−Se(5) [100.5(2)°] and Se(4)−Tl(4)−Se(5) [102.2(1)°] angles are more compressed as a result of a fourth contact to Tl(5) at both Se(3) and Se(4). The smallest Tl−Se−Tl and Se−Tl−Se angles occur in the trigonal bipyramidal Tl_2Se_3 unit comprising Tl(4) and Tl(5) in the axial positions and Se(3), Se(4), and Se(5) in the equatorial positions. These angles range from 66.40(8)° to 68.65(11)° for Tl−Se−Tl and from 83.3(1)° to 105.4(1)° for Se−Tl−Se and are even smaller than the M−Se−M and Se−M−Se angles in the trigonal bipyramidal $M_2Se_3^{2-}$ (M = Sn, Pb) anions [Sn, 71.1(1)° and 89.6(2)°; Pb, 70.7(2)° and 89.2(4)°, respectively].[16,25] The small Tl−Se−Tl bond angles within the Tl_2Se_3 unit are in accord with a Tl(4)···Tl(5) distance [3.174(2) Å] that is significantly shorter than other $Tl^I\cdots Tl^{III}$ distances [Tl(1)···Tl(4), 3.702(3) Å; Tl(2)···Tl(4), 3.726(2) Å], the $Tl^I\cdots Tl^I$ distances [Tl(1)···Tl(2), 4.007(2) Å; Tl(1)···Tl(3), 3.940(3) Å; Tl(2)···Tl(3), 3.940(2) Å] within the distorted cube, and that between Tl(3) and Tl(5) [3.602(3) Å]. The Tl(3)···Tl(5) contact is also significantly shorter than the Tl···Tl distances within the cube and is comparable to the $Tl^I\cdots Tl^I$ distances in the $Tl_2Se_2^{2-}$ [3.698(2) Å][2] and $Tl_2(Se_2C_2(CN)_2)_2^{2-}$ [3.547(4) Å][22] anions.

Solution Characterization of the $Tl_4Se_5^{4-}$ and $Tl_4Se_6^{4-}$ Anions by NMR Spectroscopy. The $Tl_4Se_5^{4-}$ and $Tl_4Se_6^{4-}$ anions were identified in en and liquid NH_3 solutions by observation of the spin-$^1/_2$ nuclides ^{205}Tl, ^{203}Tl, and ^{77}Se at their natural abundance levels and at the 94.4% ^{77}Se-enrichment level (in liquid NH_3 only). The variable temperature ^{205}Tl and ^{203}Tl NMR spectra of liquid NH_3 extracts of KTlSe and KTl^{77}Se were recorded over the temperature range −20 to −70 °C, while those of the en extract of natural abundance KTlSe were studied at 0 and 30 °C. The ^{77}Se NMR spectra of the liquid NH_3 extracts of the KTlSe and KTl^{77}Se were recorded at 0, −20, and −70 °C. Key experimental ^{205}Tl, ^{203}Tl, and ^{77}Se NMR spectra are depicted in Figures 3−10. The chemical shifts and spin−spin coupling constants, J, are summarized in Table 3. The number of observed environments, the multiplet patterns arising from $^2J(^{203(5)}Tl-^{205(3)}Tl)$ and $^1J(^{77}Se-^{205(3)}Tl)$, the satellite spacings corresponding to $^2J(^{205}Tl-^{203}Tl)$, $^1J(^{205(3)}Tl-^{77}Se)$, and $^3J(^{205(3)}Tl-^{77}Se)$, and the satellite to central peak intensity ratios, I_s/I_c, are consistent with the cubanoid $Tl_4Se_5^{4-}$ (structure **I**) and $Tl_4Se_6^{4-}$

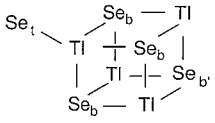

Structure I

(structure **II**) anions having C_{3v} and C_{2v} point symmetries,

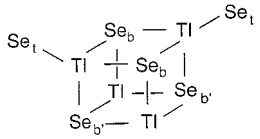

Structure II

respectively. The geometries of the $Tl_4Se_5^{4-}$ and $Tl_4Se_6^{4-}$ anions deduced from solution NMR studies are supported by the crystal structure of the related cubanoid anion, $Tl_5Se_5^{3-}$ (see X-ray Crystal Structure of (2,2,2-crypt-K^+)$_3Tl_5Se_5^{3-}$).

In addition to the previously reported $TlSe_3^{3-}$ [8] (2844 ppm at −70 °C, 2804 ppm at −20 °C) and $Tl_2Se_2^{2-}$ [2,8] (7595 ppm at −70 °C, too broad to be accurately measured at −20 °C) anions, the ^{205}Tl and ^{203}Tl NMR spectra of the red NH_3 extract

(23) Brown, I. D. *Chem. Soc. Rev.* **1978**, *7*, 359.
(24) Brown, I. D. In *Structure and Bonding in Crystals*; Academic Press: New York; 1981; Vol. II, pp 1−30.
(25) Björgvinsson, M.; Sawyer, J. F.; Schrobilgen, G. J. *Inorg. Chem.* **1987**, *26*, 741.

Table 3. Chemical Shifts (ppm) and Spin−Spin Coupling Constants (Hz) for the $Tl_4Se_5^{4-}$, $Tl_4Se_6^{4-}$, and $Tl_3Se_y^{n-}$ Anions[a]

	chemical shift ppm			spin−spin coupling constants, Hz						
					intra					
		$^{205(3)}$Tl		inter	^{205}Tl−^{203}Tl		^{205}Tl−^{77}Se[c]			
anion	^{77}Se	Tl^{I}	Tl^{III}	^{205}Tl−$^{205(3)}$Tl[b]	Tl^{I}−Tl^{I}	Tl^{III}−Tl^{III}	Tl^{I}−^{77}Se	Tl^{III}−^{77}Se	solvent	T (°C)
$Tl_4Se_5^{4-}$	−548 ($Se_{b'}$)	5531		6272 [6227]	2549		600 ($Se_{b'}$)	7537 [7645] (Se_t)	NH_3	−70
	−143 (Se_b)		1472	6279			240 (Se_b)	3928 [3958] (Se_b)		
	250 (Se_t)						150 (Se_t, ^3J)	100 ($Se_{b'}$, ^3J)		
							70 (Se_b, ^3J)			
	−530 ($Se_{b'}$)	5558		6310 [6262]	2508				NH_3	−60
	−142 (Se_b)		1467	6299 [6284]						
	245 (Se_t)									
			1457	6390				3949	NH_3	−50
		5600		6381 [6357]	2531				NH_3	−40
			1445	6456				3978		
		5424		4362					en	0
			1714[d]	4450						
		5470[d]							en	30
$Tl_4Se_6^{4-}$		5351		3682	4270				NH_3	−60
			1720							
			1705	3689		1495			NH_3	−50
		5395		3694 [3672]	4443				NH_3	−40
			1695	3699		1522				
	−88 ($Se_{b'}$)	5433		3721 [3684]	4536		∼400 ($Se_{b'}$)	8735 [8650] (Se_t)	NH_3	−20
	272 (Se_t)		1680	3738 [3682]		1538	∼600 (Se_b)	3050 [3080] (Se_b)		
	364 (Se_b)						∼150 (Se_t,^3J)	4254 [4400] ($Se_{b'}$)		
							∼70 (Se_b,^3J)	∼50 ($Se_{b'}$,^3J)		
	−79 ($Se_{b'}$)							8774 (Se_t)	NH_3	0
	280 (Se_t)							2925 (Se_b)		
	376 (Se_b)							4178 ($Se_{b'}$)		
		5110		2392	4230				en	0
			1867	2390		1615				
	−96 ($Se_{b'}$)[d]	5156		2624	4390			8364 (Se_t)	en	30
	254 (Se_t)[d]		1851	2610		1630		2272 (Se_b)		
	409 (Se_b)[d]							∼5200 ($Se_{b'}$)		
$Tl_3Se_x^{n-}$		5258			3628				en	0
			1876		3576	1312				
		5215[d]							en	30

[a] The symbols b′, b, and t denote the bridging and terminal selenium environments as defined in structures **I** and **II**. [b] Values in brackets were obtained from the ^{203}Tl spectrum. [c] Values in brackets were obtained from the ^{77}Se spectra. [d] Broad peak.

of KTlSe and KTl^{77}Se in the presence of 2,2,2-crypt consisted of a doublet (5531 ppm) and a quartet (1472 ppm) at −70 °C and two triplets (5433 and 1680 ppm) at −20 °C. At an intermediate temperature (−40 °C), both sets of new resonances were observed in approximately equal proportions (5600 and 1445 ppm; 5395 and 1695 ppm). The two triplets began to decrease in intensity at −50 and −60 °C and vanished at −70 °C. The ^{77}Se spectra consisted of a quartet (−548 ppm) and two doublets (−143 and 250 ppm) at −70 °C and two doublets (−88 and 272 ppm) and a triplet (364 ppm) at −20 °C in addition to resonances corresponding to the known $TlSe_3^{3-}$ (137 ppm, −70 °C; 148 ppm, −20 °C), $Tl_2Se_2^{2-}$ (371 ppm, −70 °C; 426 ppm, −20 °C), and Se^{2-} (−424 ppm, −70 °C; −439 ppm, −20 °C) anions. Although the triplet at 364 ppm severely overlapped the signal associated with the $Tl_2Se_2^{2-}$ anion resonance (Figure 6), it was confirmed by recording the ^{77}Se spectrum of the KTlSe extract in en at 30 °C (vide infra).

The ^{205}Tl NMR spectra of the red en extract of KTlSe in the presence of 2,2,2-crypt consisted of two doublets (∼5424 and 1876 ppm), a very broad quartet (∼1714 ppm), and three triplets (5258, 5110, and 1867 ppm) at 0 °C and of two well-defined triplets (5156 and 1851 ppm) at 30 °C. In addition, very broad signals were observed at 30 °C at ∼5470 and ∼5215 ppm (Table 3). The ^{77}Se spectrum was comprised of a singlet assigned to Se^{2-} (−433 ppm) and a triplet (409 ppm) and two doublets (254 and −96 ppm) at 30 °C. Only Se^{2-} (−427 ppm), $TlSe_3^{3-}$ (171 ppm), and $Tl_2Se_2^{2-}$ (385 Hz) could be assigned with certainty at 0 °C, while other peaks present were too weak or too broad to provide structural information. The new resonances belonging to the $Tl_4Se_5^{4-}$, $Tl_4Se_6^{4-}$, and $Tl_3Se_x^{y-}$ anions were confirmed by spectral simulations and are assigned in Table 3. The derivations of their solution structures are discussed in detail below.

Determination of the Solution Structures of the $Tl_4Se_5^{4-}$, $Tl_4Se_6^{4-}$, and $Tl_3Se_x^{y-}$ Anions. The solution structures of the title anions have been deduced from detailed analyses and simulations of their component subspectra and accompanying spin−spin coupling patterns in their ^{77}Se, ^{203}Tl, and ^{205}Tl spectra. The ^{205}Tl and ^{203}Tl NMR spectra of the natural abundance and ^{77}Se-enriched $Tl_4Se_5^{4-}$ and $Tl_4Se_6^{4-}$ anions were simulated using the computer program ISOTOPOMER,[26] the natural and enriched abundances of the spin-$^1/_2$ nuclides [^{205}Tl (70.5%), ^{203}Tl (29.5%), and ^{77}Se (7.58%; isotopically enriched, 94.4%)], and the values of the observed coupling constants. Although the entire manifold of isotopomeric subspectra (e.g., 637 absolute isotopomers were used to simulate the ^{203}Tl NMR spectrum of $Tl_4Se_6^{4-}$) was summed to simulate the ^{205}Tl and ^{203}Tl NMR spectra, Tables 4 and 5 list only the abundances and multiplicities of the isotopomers having fractional abundances ≥0.0001. The resulting simulations (Figures 4, 5, 7, 8) are in excellent agreement with the experimental spectra and account for all

(26) Santry, D. P.; Mercier, H. P. A.; Schrobilgen, G. J. *ISOTOPOMER, A Multi-NMR Simulation Program*, version 3.02NTF.; Snowbird Software, Inc.: Hamilton, ON, 2000.

Table 4. The Most Abundant Natural Abundance and ^{77}Se-Enriched Isotopomers and Subspectra Comprising the ^{205}Tl and ^{203}Tl NMR Spectra of the $Tl_4Se_5^{4-}$ Anion

Natural Abundance

$^{205}Tl_x^{III}\,^{203}Tl_{1-x}^{III}\,^{205}Tl_y^{I}\,^{203}Tl_{3-y}^{I}$ $^{77}Se_z\,^{0}Se_{5-z}^{4-\,a}$			isotopomer fractional abundance,[b]	multiplicity observed for the components of the subspectra in the Tl^{III} Region[c]		$^{205}Tl_x^{III}\,^{203}Tl_{1-x}^{III}\,^{205}Tl_y^{I}\,^{203}Tl_{3-y}^{I}$ $^{77}Se_z\,^{0}Se_{5-z}^{4-\,a}$			isotopomer fractional abundance,[b]	multiplicity observed for the components of the subspectra in the Tl^{I} Region[c]	
x	y	z ^{77}Se environments		^{205}Tl	^{203}Tl	x	y	z ^{77}Se environments		^{205}Tl	^{203}Tl
1	3	0	0.1666	Q	-	1	3	0	0.1666	D	-
1	2	0	0.2091			0	3	0	0.0697		
1	1	0	0.0875								
1	0	0	0.0122			1	2	0	0.2091	$D/^2d_{Tl^I}^{Tl^I}$	$D/^2t_{Tl^I}^{Tl^I}$
						0	2	0	0.0875		
1	3	1 (Se_b)	0.0410	$Q/^1d_{Se_b}^{Tl^{III}}$	-						
1	2	1 "	0.0514			1	1	0	0.0875	$D/^2t_{Tl^I}^{Tl^I}$	$D/^2d_{Tl^I}^{Tl^I}$
1	1	1 "	0.0215			0	1	0	0.0366		
1	0	1 "	0.0030								
						1	0	0	0.0122	-	D
1	3	1 ($Se_{b'}$)	0.0137	$Q/^3d_{Se_{b'}}^{Tl^{III}}$	-	0	0	0	0.0051		
1	2	1 "	0.0171								
1	1	1 "	0.0072			1	3	1 (Se_b)	0.0410	$D/^1d_{Se_b}^{Tl^I}$	-
1	0	1 "	0.0010			0	3	1 "	0.0172		
1	3	1 (Se_t)	0.0137	$Q/^1d_{Se_t}^{Tl^{III}}$	-	1	2	1 (Se_b)	0.0171	$D/^2d_{Tl^I}^{Tl^I}/^3d_{Se_b}^{Tl^I}$	$D/^2t_{Tl^I}^{Tl^I}/^3d_{Se_b}^{Tl^I}$
1	2	1 "	0.0171			0	2	1 "	0.0072		
1	1	1 "	0.0072								
1	0	1 "	0.0010			1	2	1 (Se_b)	0.0343	$D/^2d_{Tl^I}^{Tl^I}/^1d_{Se_b}^{Tl^I}$	$D/^2t_{Tl^I}^{Tl^I}/^1d_{Se_b}^{Tl^I}$
						0	2	1 "	0.0144		
0	3	0	0.0697	-	Q						
0	2	0	0.0875			1	1	1 (Se_b)	0.0072	$D/^2t_{Tl^I}^{Tl^I}/^3d_{Se_b}^{Tl^I}$	$D/^2d_{Tl^I}^{Tl^I}/^3d_{Se_b}^{Tl^I}$
0	1	0	0.0366			0	1	1 "	0.0030		
0	0	0	0.0051								
						1	1	1 (Se_b)	0.0144	$D/^2t_{Tl^I}^{Tl^I}/^1d_{Se_b}^{Tl^I}$	$D/^2d_{Tl^I}^{Tl^I}/^1d_{Se_b}^{Tl^I}$
0	3	1 (Se_b)	0.0171	-	$Q/^1d_{Se_b}^{Tl^{III}}$	0	1	1 "	0.0060		
0	2	1 "	0.0215								
0	1	1 "	0.0090			1	0	1 (Se_b)	0.0030	-	$D/^1d_{Se_b}^{Tl^I}$
0	0	1 "	0.0013			0	0	1 "	0.0013		
0	3	1 ($Se_{b'}$)	0.0057	-	$Q/^3d_{Se_{b'}}^{Tl^{III}}$	1	3	1 ($Se_{b'}$)	0.0137	$D/^1d_{Se_{b'}}^{Tl^I}$	-
0	2	1 "	0.0072			0	3	1 "	0.0057		
0	1	1 "	0.0030								
0	0	1 "	0.0004			1	2	1 ($Se_{b'}$)	0.0171	$D/^2d_{Tl^I}^{Tl^I}/^1d_{Se_{b'}}^{Tl^I}$	$D/^2t_{Tl^I}^{Tl^I}/^1d_{Se_{b'}}^{Tl^I}$
						0	2	1 "	0.0072		
0	3	1 (Se_t)	0.0057	-	$Q/^1d_{Se_t}^{Tl^{III}}$						
0	2	1 "	0.0072			1	1	1 ($Se_{b'}$)	0.0072	$D/^2t_{Tl^I}^{Tl^I}/^1d_{Se_{b'}}^{Tl^I}$	$D/^2d_{Tl^I}^{Tl^I}/^1d_{Se_{b'}}^{Tl^I}$
0	1	1 "	0.0030			0	1	1 "	0.0030		
0	0	1 "	0.0004								
						1	0	1 ($Se_{b'}$)	0.0010	-	$D/^1d_{Se_{b'}}^{Tl^I}$
						0	0	1 "	0.0004		
						1	3	1 (Se_t)	0.0137	$D/^1d_{Se_t}^{Tl^I}$	-
						0	3	1 "	0.0057		
						1	2	1 (Se_t)	0.0171	$D/^2d_{Tl^I}^{Tl^I}/^1d_{Se_t}^{Tl^I}$	$D/^2t_{Tl^I}^{Tl^I}/^1d_{Se_t}^{Tl^I}$
						0	2	1 "	0.0072		
						1	1	1 (Se_t)	0.0072	$D/^2t_{Tl^I}^{Tl^I}/^1d_{Se_t}^{Tl^I}$	$D/^2d_{Tl^I}^{Tl^I}/^1d_{Se_t}^{Tl^I}$
						0	1	1 "	0.0030		
						1	0	1 (Se_t)	0.0010	-	$D/^1d_{Se_t}^{Tl^I}$
						0	0	1 "	0.0004		

^{77}Se enriched

$^{205}Tl_x^{III}\,^{203}Tl_{1-x}^{III}\,^{205}Tl_y^{I}\,^{203}Tl_{3-y}^{I}$ $^{77}Se_z\,^{0}Se_{5-z}^{4-\,a}$			isotopomer fractional abundance,[b]	multiplicity observed for the components of the subspectra in the Tl^{III} Region		$^{205}Tl_x^{III}\,^{203}Tl_{1-x}^{III}\,^{205}Tl_y^{I}\,^{203}Tl_{3-y}^{I}$ $^{77}Se_z\,^{0}Se_{5-z}^{4-\,a}$			isotopomer fractional abundance,[b]	multiplicity observed for the components of the subspectra in the Tl^{I} Region	
x	y	z ^{77}Se environments		^{205}Tl	^{203}Tl	x	y	z ^{77}Se environments		^{205}Tl	^{203}Tl
1	3	5 ($3Se_b$, $Se_{b'}$, Se_t)	0.1852	$Q/^1d_{Se_t}^{Tl^{III}}/^1q_{Se_b}^{Tl^{III}}/^1d_{Se_{b'}}^{Tl^{III}}$	-	1	3	5 ($3Se_b$, $Se_{b'}$, Se_t)	0.1852	$D/^1d_{Se_{b'}}^{Tl^I}/^1t_{Se_b}^{Tl^I}/$	-
1	2	5 "	0.2325			0	3	5 "	0.0775	$^3d_{Se_b}^{Tl^I}/^3d_{Se_t}^{Tl^I}$	
1	1	5 "	0.0973								
1	0	5 "	0.0136			1	2	5 "	0.2325	$D/^2d_{Tl^I}^{Tl^I}/^1d_{Se_{b'}}^{Tl^I}/$	$D/^2t_{Tl^I}^{Tl^I}/^1d_{Se_{b'}}^{Tl^I}/$
						0	2	5 "	0.0973	$^1t_{Se_b}^{Tl^I}/^3d_{Se_b}^{Tl^I}/^3d_{Se_t}^{Tl^I}$	$^1t_{Se_b}^{Tl^I}/^3d_{Se_b}^{Tl^I}/^3d_{Se_t}^{Tl^I}$
1	3	4 ($2Se_b$, $Se_{b'}$, Se_t)	0.0330	$Q/^1d_{Se_t}^{Tl^{III}}/^1t_{Se_b}^{Tl^{III}}/^1d_{Se_{b'}}^{Tl^{III}}$	-						
1	2	4 "	0.0414			1	1	5 "	0.0973	$D/^2t_{Tl^I}^{Tl^I}/^1d_{Se_{b'}}^{Tl^I}/$	$D/^2d_{Tl^I}^{Tl^I}/^1d_{Se_{b'}}^{Tl^I}/$
1	1	4 "	0.0173			0	1	5 "	0.0407	$^1t_{Se_b}^{Tl^I}/^3d_{Se_b}^{Tl^I}/^3d_{Se_t}^{Tl^I}$	$^1t_{Se_b}^{Tl^I}/^3d_{Se_b}^{Tl^I}/^3d_{Se_t}^{Tl^I}$
1	0	4 "	0.0024								

Table 4 (Continued)

$^{205}Tl_x^{III}\,^{203}Tl_{1-x}^{III}\,^{205}Tl_y^{I}\,^{203}Tl_{3-y}^{I}\,^{77}Se_z\,^{0}Se_{5-z}^{4-a}$				isotopomer fractional abundance,[b]	multiplicity observed for the components of the subspectra in the Tl^{III} Region	
x	y	z	^{77}Se environments		^{205}Tl	^{203}Tl
			^{77}Se enriched			
1	3	4	($3Se_b$, Se_t)	0.0110	$Q/{}^1d^{Tl^{III}}_{Se_t}/{}^1q^{Tl^{III}}_{Se_b}$	-
1	2	4	"	0.0138		
1	1	4	"	0.0058		
1	0	4	"	0.0008		
1	3	4	($3Se_b$, $Se_{b'}$)	0.0110	$Q/{}^1q^{Tl^{III}}_{Se_b}/{}^1d^{Tl^{III}}_{Se_{b'}}$	-
1	2	4	"	0.0138		
1	1	4	"	0.0058		
1	0	4	"	0.0008		
0	3	5	($3Se_b$, $Se_{b'}$, Se_t)	0.0775	- $Q/{}^1d^{Tl^{III}}_{Se_t}/{}^1q^{Tl^{III}}_{Se_b}/{}^1d^{Tl^{III}}_{Se_{b'}}$	
0	2	5	"	0.0973		
0	1	5	"	0.0407		
0	0	5	"	0.0057		
0	3	4	($2Se_b$, $Se_{b'}$, Se_t)	0.0138	- $Q/{}^1d^{Tl^{III}}_{Se_t}/{}^1t^{Tl^{III}}_{Se_b}/{}^1d^{Tl^{III}}_{Se_{b'}}$	
0	2	4	"	0.0173		
0	1	4	"	0.0072		
0	0	4	"	0.0011		
0	3	4	($3Se_b$, Se_t)	0.0046	- $Q/{}^1d^{Tl^{III}}_{Se_t}/{}^1q^{Tl^{III}}_{Se_b}$	
0	2	4	"	0.0058		
0	1	4	"	0.0024		
0	0	4	"	0.0003		
0	3	4	($3Se_b$, $Se_{b'}$)	0.0046	- $Q/{}^1q^{Tl^{III}}_{Se_b}/{}^1d^{Tl^{III}}_{Se_{b'}}$	
0	2	4	"	0.0058		
0	1	4	"	0.0024		
0	0	4	"	0.0003		
1	0	5	"	0.0136	-	$D/{}^1d^{Tl^I}_{Se_{b'}}/{}^1t^{Tl^I}_{Se_b}/{}^3d^{Tl^I}_{Se_b}/{}^3d^{Tl^I}_{Se_t}$
0	0	5	"	0.0057		
1	3	4	($2Se_b$, $Se_{b'}$, Se_t)	0.0330	$D/{}^1d^{Tl^I}_{Se_{b'}}/{}^1d^{Tl^I}_{Se_b}/{}^3d^{Tl^I}_{Se_b}/{}^3d^{Tl^I}_{Se_t}$	-
0	3	4	"	0.0138		
1	2	4	"	0.0184	$D/{}^2d^{Tl^I}_{Tl^I}/{}^1d^{Tl^I}_{Se_{b'}}/{}^1t^{Tl^I}_{Se_b}/{}^3d^{Tl^I}_{Se_t}$	$D/{}^2t^{Tl^I}_{Tl^I}/{}^1d^{Tl^I}_{Se_{b'}}/{}^1t^{Tl^I}_{Se_b}/{}^3d^{Tl^I}_{Se_t}$
0	2	4	"	0.0077		
1	2	4	"	0.0230	$D/{}^2d^{Tl^I}_{Tl^I}/{}^1d^{Tl^I}_{Se_{b'}}/{}^1d^{Tl^I}_{Se_b}/{}^3d^{Tl^I}_{Se_b}/{}^3d^{Tl^I}_{Se_t}$	$D/{}^2t^{Tl^I}_{Tl^I}/{}^1d^{Tl^I}_{Se_{b'}}/{}^1d^{Tl^I}_{Se_b}/{}^3d^{Tl^I}_{Se_b}/{}^3d^{Tl^I}_{Se_t}$
0	2	4	"	0.0096		
1	1	4	"	0.0077	$D/{}^2t^{Tl^I}_{Tl^I}/1d^{Tl^I}_{Se_{b'}}/{}^1t^{Tl^I}_{Se_b}/{}^3d^{Tl^I}_{Se_t}$	$D/{}^2d^{Tl^I}_{Tl^I}/{}^1d^{Tl^I}_{Se_{b'}}/{}^1t^{Tl^I}_{Se_b}/{}^3d^{Tl^I}_{Se_t}$
0	1	4	"	0.0032		
1	1	4	"	0.0096	$D/{}^2t^{Tl^I}_{Tl^I}/{}^1d^{Tl^I}_{Se_{b'}}/{}^1d^{Tl^I}_{Se_b}/{}^3d^{Tl^I}_{Se_b}/{}^3d^{Tl^I}_{Se_t}$	$D/{}^2d^{Tl^I}_{Tl^I}/{}^1d^{Tl^I}_{Se_{b'}}/{}^1d^{Tl^I}_{Se_b}/{}^3d^{Tl^I}_{Se_b}/{}^3d^{Tl^I}_{Se_t}$
0	1	4	"	0.0042		
1	0	4	"	0.0024	-	$D/{}^1d^{Tl^I}_{Se_{b'}}/{}^1d^{Tl^I}_{Se_b}/{}^3d^{Tl^I}_{Se_b}/{}^3d^{Tl^I}_{Se_t}$
0	0	4	"	0.0010		
1	3	4	($3Se_b$, Se_t)	0.0110	$D/{}^1t^{Tl^I}_{Se_b}/{}^3d^{Tl^I}_{Se_b}/{}^3d^{Tl^I}_{Se_t}$	
0	3	4	"	0.0046		-
1	2	4	"	0.0138	$D/{}^2d^{Tl^I}_{Tl^I}/{}^1t^{Tl^I}_{Se_b}/{}^3d^{Tl^I}_{Se_b}/{}^3d^{Tl^I}_{Se_t}$	$D/{}^2t^{Tl^I}_{Tl^I}/{}^1t^{Tl^I}_{Se_b}/{}^3d^{Tl^I}_{Se_b}/{}^3d^{Tl^I}_{Se_t}$
0	2	4	"	0.0058		
1	1	4	"	0.0058	$D/{}^2t^{Tl^I}_{Tl^I}/{}^1t^{Tl^I}_{Se_b}/{}^3d^{Tl^I}_{Se_b}/{}^3d^{Tl^I}_{Se_t}$	$D/{}^2d^{Tl^I}_{Tl^I}/{}^1t^{Tl^I}_{Se_b}/{}^3d^{Tl^I}_{Se_b}/{}^3d^{Tl^I}_{Se_t}$
0	1	4	"	0.0024		
1	0	4	"	0.0008	-	$D/{}^1t^{Tl^I}_{Se_b}/{}^3d^{Tl^I}_{Se_b}/{}^3d^{Tl^I}_{Se_t}$
0	0	4	"	0.0003		
1	3	4	($3Se_b$, $Se_{b'}$)	0.0110	$D/{}^1d^{Tl^I}_{Se_{b'}}/{}^3t^{Tl^I}_{Se_b}/{}^3d^{Tl^I}_{Se_t}$	-
0	3	4	"	0.0046		
1	2	4	"	0.0138	$D/{}^2d^{Tl^I}_{Tl^I}/{}^1d^{Tl^I}_{Se_{b'}}/{}^3t^{Tl^I}_{Se_b}/{}^3d^{Tl^I}_{Se_t}$	$D/{}^2t^{Tl^I}_{Tl^I}/{}^1d^{Tl^I}_{Se_{b'}}/{}^3t^{Tl^I}_{Se_b}/{}^3d^{Tl^I}_{Se_t}$
0	2	4	"	0.0058		
1	1	4	"	0.0058	$D/{}^2t^{Tl^I}_{Tl^I}/{}^1d^{Tl^I}_{Se_{b'}}/{}^3t^{Tl^I}_{Se_b}/{}^3d^{Tl^I}_{Se_t}$	$D/{}^2d^{Tl^I}_{Tl^I}/{}^1d^{Tl^I}_{Se_{b'}}/{}^3t^{Tl^I}_{Se_b}/{}^3d^{Tl^I}_{Se_t}$
0	1	4	"	0.0024		
1	0	4	"	0.0008	-	$D/{}^1d^{Tl^I}_{Se_{b'}}/{}^3t^{Tl^I}_{Se_b}/{}^3d^{Tl^I}_{Se_t}$
0	0	4	"	0.0003		

[a] ^{0}Se denotes spinless selenium atoms. [b] Natural abundances of the spin-$^1/_2$ nuclides used to calculate isotopomer fractional abundances were taken from ref 27: ^{77}Se (natural abundance, 7.58%; enriched, 94.4%); ^{203}Tl, 29.5%; ^{205}Tl, 70.5%. Although all isotopomers were included in the simulations, only isotopomer fractional abundances ≥0.0001 are listed in the table. [c] Capital letters Q (quartet), D (doublet), and T (triplet) denote interenvironmental couplings arising from $J(^{205}Tl^{III}-^{203}Tl^{I})$ or $J(^{205}Tl^{III}-^{205}Tl^{I})$ that cannot be distinguished because of the small difference in absolute frequency between the ^{205}Tl and ^{203}Tl nuclides. Lower case letters q (quartet), d (doublet), and t (triplet) denote satellite couplings arising from $J(^{205}Tl-^{203}Tl)$ or $J(^{205(3)}Tl-^{77}Se)$. The left superscript denotes the order of the J coupling; the right superscript and subscript denote the two nuclei that are spin coupled. For example, the description $D/{}^2d^{Tl^I}_{Tl^I}/{}^1d^{Tl^I}_{Se_b}$ denotes a doublet-of-doublets-of doublets that results from unresolved doublets arising from $^2J(^{205}Tl^{I}-^{203}Tl^{III})$ and $^2J(^{205}Tl^{I}-^{205}Tl^{III})$; each component of the DOUBLET is split into doublet satellites originating from $^2J(^{205}Tl^{I}-^{203}Tl^{I})$ and $^1J(^{205}Tl^{I}-^{77}Se_b)$. Each multiplicity description refers to a single set of selenium environments and its associated isotopomers.

the observed peaks and minor asymmetries arising from second-order effects that result from the relatively small difference in absolute frequencies (0.562 MHz)[27] between coupled ^{203}Tl and ^{205}Tl nuclei and the large ^{205}Tl−^{203}Tl, ^{205}Tl−^{205}Tl, and ^{203}Tl−

Table 5. The Most Abundant Natural Abundance and ^{77}Se-Enriched Isotopomers and Subspectra Comprising the ^{205}Tl and ^{203}Tl NMR Spectra of the $Tl_4Se_6^{4-}$ Anion[a]

Natural Abundance

$^{205}Tl_x^{III}\,^{203}Tl_{2-x}^{III}\,^{205}Tl_y^{I}\,^{203}Tl_{2-y}^{I}$ $^{77}Se_z\,^{0}Se_{6-z}^{4-}$[a]				isotopomer fractional abundance,[b]	multiplicity of the components of the subspectra in the Tl^{III} Region[c]	
x	y	z	^{77}Se environments		^{205}Tl	^{203}Tl
2	2	0		0.1539	T	-
2	1	0		0.1288		
2	0	0		0.0270		
2	2	1	(Se_t)	0.0253	$T/{}^1d_{Se_t}^{Tl^{III}}/{}^3d_{Se_t}^{Tl^{III}}$	-
2	1	1	"	0.0211		
2	0	1	"	0.0044		
2	2	1	(Se_b)	0.0253	$T/{}^1d_{Se_b}^{Tl^{III}}$	-
2	1	1	"	0.0211		
2	0	1	"	0.0044		
2	2	1	($Se_{b'}$)	0.0253	$T/{}^1d_{Se_{b'}}^{Tl^{III}}/{}^3d_{Se_{b'}}^{Tl^{III}}$	-
2	1	1	"	0.0211		
2	0	1	"	0.0044		
1	2	0		0.1288	$T/{}^2d_{Tl^{III}}^{Tl^{III}}$	$T/{}^2d_{Tl^{III}}^{Tl^{III}}$
1	1	0		0.1078		
1	0	0		0.0226		
1	2	1	(Se_t)	0.0106	$T/{}^2d_{Tl^{III}}^{Tl^{III}}/{}^1d_{Se_t}^{Tl^{III}}$	$T/{}^2d_{Tl^{III}}^{Tl^{III}}/{}^1d_{Se_t}^{Tl^{III}}$
1	1	1	"	0.0088		
1	0	1	"	0.0019		
1	2	1	(Se_t)	0.0106	$T/{}^2d_{Tl^{III}}^{Tl^{III}}/{}^3d_{Se_t}^{Tl^{III}}$	$T/{}^2d_{Tl^{III}}^{Tl^{III}}/{}^3d_{Se_t}^{Tl^{III}}$
1	1	1	"	0.0088		
1	0	1	"	0.0019		
1	2	1	(Se_b)	0.0211	$T/{}^2d_{Tl^{III}}^{Tl^{III}}/{}^1d_{Se_b}^{Tl^{III}}$	$T/{}^2d_{Tl^{III}}^{Tl^{III}}/{}^1d_{Se_b}^{Tl^{III}}$
1	1	1	"	0.0177		
1	0	1	"	0.0037		
1	2	1	($Se_{b'}$)	0.0106	$T/{}^2d_{Tl^{III}}^{Tl^{III}}/{}^1d_{Se_{b'}}^{Tl^{III}}$	$T/{}^2d_{Tl^{III}}^{Tl^{III}}/{}^1d_{Se_{b'}}^{Tl^{III}}$
1	1	1	"	0.0088		
1	0	1	"	0.0019		
1	2	1	($Se_{b'}$)	0.0106	$T/{}^2d_{Tl^{III}}^{Tl^{III}}/{}^3d_{Se_{b'}}^{Tl^{III}}$	$T/{}^2d_{Tl^{III}}^{Tl^{III}}/{}^3d_{Se_{b'}}^{Tl^{III}}$
1	1	1	"	0.0088		
1	0	1	"	0.0019		
0	2	0		0.0270	-	T
0	1	0		0.0226		
0	0	0		0.0047		
0	2	1	(Se_t)	0.0044	-	$T/{}^1d_{Se_t}^{Tl^{III}}/{}^3d_{Se_t}^{Tl^{III}}$
0	1	1	"	0.0037		
0	0	1	"	0.0008		
0	2	1	(Se_b)	0.0044	-	$T/{}^1d_{Se_b}^{Tl^{III}}$
0	1	1	"	0.0037		
0	0	1	"	0.0008		
0	2	1	($Se_{b'}$)	0.0044	-	$T/{}^1d_{Se_{b'}}^{Tl^{III}}/{}^3d_{Se_{b'}}^{Tl^{III}}$
0	1	1	"	0.0037		
0	0	1	"	0.0008		

$^{205}Tl_x^{III}\,^{203}Tl_{2-x}^{III}\,^{205}Tl_y^{I}\,^{203}Tl_{2-y}^{I}$ $^{77}Se_z\,^{0}Se_{6-z}^{4-}$[a]				isotopomer fractional abundance,[b]	multiplicity of the components of the subspectra in the Tl^{I} Region[c]	
x	y	z	^{77}Se environments		^{205}Tl	^{203}Tl
2	2	0		0.1539	T	-
1	2	0		0.1288		
0	2	0		0.0270		
2	2	1	(Se_t)	0.0253	$T/{}^3d_{Se_t}^{Tl^{I}}$	-
1	2	1	"	0.0211		
0	2	1	"	0.0044		
2	2	1	(Se_b)	0.0253	$T/{}^1d_{Se_b}^{Tl^{I}}/{}^3d_{Se_b}^{Tl^{I}}$	-
1	2	1	"	0.0211		
0	2	1	"	0.0044		
2	2	1	($Se_{b'}$)	0.0253	$T/{}^1d_{Se_{b'}}^{Tl^{I}}$	-
1	2	1	"	0.0211		
0	2	1	"	0.0044		
2	1	0		0.1288	$T/{}^2d_{Tl^{I}}^{Tl^{I}}$	$T/{}^2d_{Tl^{I}}^{Tl^{I}}$
1	1	0		0.1078		
0	1	0		0.0226		
2	1	1	(Se_t)	0.0211	$T/{}^2d_{Tl^{I}}^{Tl^{I}}/{}^3d_{Se_t}^{Tl^{I}}$	$T/{}^2d_{Tl^{I}}^{Tl^{I}}/{}^3d_{Se_t}^{Tl^{I}}$
1	1	1	"	0.0177		
0	1	1	"	0.0037		
2	1	1	(Se_b)	0.0106	$T/{}^2d_{Tl^{I}}^{Tl^{I}}/{}^1d_{Se_b}^{Tl^{I}}$	$T/{}^2d_{Tl^{I}}^{Tl^{I}}/{}^1d_{Se_b}^{Tl^{I}}$
1	1	1	"	0.0088		
0	1	1	"	0.0019		
2	1	1	($Se_{b'}$)	0.0211	$T/{}^2d_{Tl^{I}}^{Tl^{I}}/{}^1d_{Se_{b'}}^{Tl^{I}}$	$T/{}^2d_{Tl^{I}}^{Tl^{I}}/{}^1d_{Se_{b'}}^{Tl^{I}}$
1	1	1	"	0.0177		
0	1	1	"	0.0037		
2	1	1	(Se_b)	0.0106	$T/{}^2d_{Tl^{I}}^{Tl^{I}}/{}^3d_{Se_b}^{Tl^{I}}$	$T/{}^2d_{Tl^{I}}^{Tl^{I}}/{}^3d_{Se_b}^{Tl^{I}}$
1	1	1	"	0.0088		
0	1	1	"	0.0019		
2	0	0		0.0270	-	T
1	0	0		0.0226		
0	0	0		0.0047		
2	0	1	(Se_t)	0.0044	-	$T/{}^3d_{Se_t}^{Tl^{I}}$
1	0	1	"	0.0037		
0	0	1	"	0.0008		
2	0	1	(Se_b)	0.0044	-	$T/{}^1d_{Se_b}^{Tl^{I}}/{}^3d_{Se_b}^{Tl^{I}}$
1	0	1	"	0.0037		
0	0	1	"	0.000		
2	0	1	($Se_{b'}$)	0.0044	-	$T/{}^1d_{Se_{b'}}^{Tl^{I}}$
1	0	1	"	0.0037		
0	0	1	"	0.0008		

^{77}Se enriched

$^{205}Tl_x^{III}\,^{203}Tl_{2-x}^{III}\,^{205}Tl_y^{I}\,^{203}Tl_{2-y}^{I}$ $^{77}Se_z\,^{0}Se_{6-z}^{4-}$[a]				isotopomer fractional abundance,[b]	multiplicity observed for the components of the subspectra in the Tl^{III} Region	
x	y	z	^{77}Se environments		^{205}Tl	^{203}Tl
2	2	6	($2Se_b$, $2Se_{b'}$, $2Se_t$)	0.1748	$T/{}^1d_{Se_t}^{Tl^{III}}/{}^1t_{Se_b}^{Tl^{III}}/$	-
2	1	6	"	0.1463	${}^1d_{Se_{b'}}^{Tl^{III}}/{}^3d_{Se_t}^{Tl^{III}}/{}^3d_{Se_{b'}}^{Tl^{III}}$	
2	0	6	"	0.0306		
2	2	5	($2Se_b$, $2Se_{b'}$, Se_t)	0.0207	$T/{}^1d_{Se_t}^{Tl^{III}}/{}^1t_{Se_b}^{Tl^{III}}/$	-
2	1	5	"	0.0174	${}^1d_{Se_{b'}}^{Tl^{III}}/{}^3d_{Se_{b'}}^{Tl^{III}}$	
2	0	5	"	0.0036		

$^{205}Tl_x^{III}\,^{203}Tl_{2-x}^{III}\,^{205}Tl_y^{I}\,^{203}Tl_{2-y}^{I}$ $^{77}Se_z\,^{0}Se_{6-z}^{4-}$[a]				isotopomer fractional abundance,[b]	multiplicity observed for the components of the subspectra in the Tl^{I} Region	
x	y	z	^{77}Se environments		^{205}Tl	^{203}Tl
2	2	6	($2Se_b$, $2Se_{b'}$, $2Se_t$)	0.1748	$T/{}^1d_{Se_b}^{Tl^{I}}/{}^1t_{Se_{b'}}^{Tl^{I}}/$	-
1	2	6	"	0.1463	${}^3t_{Se_t}^{Tl^{I}}/{}^3d_{Se_b}^{Tl^{I}}$	
0	2	6	"	0.0306		
2	2	5	($2Se_b$, $2Se_{b'}$, Se_t)	0.0207	$T/{}^1d_{Se_b}^{Tl^{I}}/{}^1t_{Se_{b'}}^{Tl^{I}}/$	-
1	2	5	"	0.0174	${}^3d_{Se_t}^{Tl^{I}}/{}^3d_{Se_b}^{Tl^{I}}$	
0	2	5	"	0.0036		

Table 5 (Continued)

$^{205}Tl_x^{III}\,^{203}Tl_{2-x}^{III}\,^{205}Tl_y^{I}\,^{203}Tl_{2-y}^{I}$ $^{77}Se_z\,^{0}Se_{6-z}^{4-\,a}$				isotopomer fractional abundance,[b]	multiplicity observed for the components of the subspectra in the Tl^{III} Region	
x	y	z	^{77}Se environments		^{205}Tl	^{203}Tl
2	2	5	(Se_b, $2Se_{b'}$, $2Se_t$)	0.0207	$T/{}^1d_{Se_t}^{Tl^{III}}/{}^1d_{Se_b}^{Tl^{III}}/{}^1d_{Se_{b'}}^{Tl^{III}}/{}^3d_{Se_t}^{Tl^{III}}/{}^3d_{Se_{b'}}^{Tl^{III}}$	-
2	1	5	"	0.0174		
2	0	5	"	0.0036		
2	2	5	($2Se_b$, $Se_{b'}$, $2Se_t$)	0.0207	$T/{}^1d_{Se_t}^{Tl^{III}}/{}^1t_{Se_b}^{Tl^{III}}/{}^1d_{Se_{b'}}^{Tl^{III}}/{}^3d_{Se_t}^{Tl^{III}}/$	-
2	1	5	"	0.0174		
2	0	5	"	0.0036		
1	2	6	($2Se_b$, $2Se_{b'}$, $2Se_t$)	0.1463	$T/{}^2d_{Tl^{III}}^{Tl^{III}}/{}^1d_{Se_t}^{Tl^{III}}/{}^1t_{Se_b}^{Tl^{III}}/{}^1d_{Se_b}^{Tl^{III}}/{}^3d_{Se_t}^{Tl^{III}}/{}^3d_{Se_{b'}}^{Tl^{III}}$	$T/{}^2d_{Tl^{III}}^{Tl^{III}}/{}^1d_{Se_t}^{Tl^{III}}/{}^1t_{Se_b}^{Tl^{III}}/{}^1d_{Se_b}^{Tl^{III}}/{}^3d_{Se_t}^{Tl^{III}}/{}^3d_{Se_{b'}}^{Tl^{III}}$
1	1	6	"	0.1224		
1	0	6	"	0.0256		
1	2	5	($2Se_b$, $2Se_{b'}$, Se_t)	0.0087	$T/{}^2d_{Tl^{III}}^{Tl^{III}}/{}^1d_{Se_t}^{Tl^{III}}/{}^1t_{Se_b}^{Tl^{III}}/{}^1d_{Se_{b'}}^{Tl^{III}}/{}^3d_{Se_{b'}}^{Tl^{III}}$	$T/{}^2d_{Tl^{III}}^{Tl^{III}}/{}^1d_{Se_t}^{Tl^{III}}/{}^1t_{Se_b}^{Tl^{III}}/{}^1d_{Se_{b'}}^{Tl^{III}}/{}^3d_{Se_{b'}}^{Tl^{III}}$
1	1	5	"	0.0073		
1	0	5	"	0.0015		
1	2	5	($2Se_b$, $2Se_{b'}$, Se_t)	0.0087	$T/{}^2d_{Tl^{III}}^{Tl^{III}}/{}^1t_{Se_b}^{Tl^{III}}/{}^1d_{Se_{b'}}^{Tl^{III}}/{}^3d_{Se_t}^{Tl^{III}}/{}^3d_{Se_{b'}}^{Tl^{III}}$	$T/{}^2d_{Tl^{III}}^{Tl^{III}}/{}^1t_{Se_b}^{Tl^{III}}/{}^1d_{Se_{b'}}^{Tl^{III}}/{}^3d_{Se_t}^{Tl^{III}}/{}^3d_{Se_{b'}}^{Tl^{III}}$
1	1	5	"	0.0073		
1	0	5	"	0.0015		
1	2	5	(Se_b, $2Se_{b'}$, $2Se_t$)	0.0174	$T/{}^2d_{Tl^{III}}^{Tl^{III}}/{}^1d_{Se_t}^{Tl^{III}}/{}^1d_{Se_b}^{Tl^{III}}/{}^1d_{Se_{b'}}^{Tl^{III}}/{}^3d_{Se_t}^{Tl^{III}}/{}^3d_{Se_{b'}}^{Tl^{III}}$	$T/{}^2d_{Tl^{III}}^{Tl^{III}}/{}^1d_{Se_t}^{Tl^{III}}/{}^1d_{Se_b}^{Tl^{III}}/{}^1d_{Se_{b'}}^{Tl^{III}}/{}^3d_{Se_t}^{Tl^{III}}/{}^3d_{Se_{b'}}^{Tl^{III}}$
1	1	5	"	0.0145		
1	0	5	"	0.0030		
1	2	5	($2Se_b$, $Se_{b'}$, $2Se_t$)	0.0087	$T/{}^2d_{Tl^{III}}^{Tl^{III}}/{}^1d_{Tl^{III}}^{Tl^{III}}/{}^1d_{Se_t}^{Tl^{III}}/{}^1t_{Se_b}^{Tl^{III}}/{}^3d_{Se_t}^{Tl^{III}}/{}^3d_{Se_{b'}}^{Tl^{III}}$	$T/{}^2d_{Tl^{III}}^{Tl^{III}}/{}^1d_{Tl^{III}}^{Tl^{III}}/{}^1d_{Se_t}^{Tl^{III}}/{}^1t_{Se_b}^{Tl^{III}}/{}^3d_{Se_t}^{Tl^{III}}/{}^3d_{Se_{b'}}^{Tl^{III}}$
1	1	5	"	0.0073		
1	0	5	"	0.0015		
0	2	6	($2Se_b$, $2Se_{b'}$, $2Se_t$)	0.0306	-	$T/{}^1d_{Se_t}^{Tl^{III}}/{}^1t_{Se_b}^{Tl^{III}}/{}^1d_{Se_{b'}}^{Tl^{III}}/{}^3d_{Se_t}^{Tl^{III}}/{}^3d_{Se_{b'}}^{Tl^{III}}$
0	1	6	"	0.0256		
0	0	6	"	0.0054		
0	2	5	($2Se_b$, $2Se_{b'}$, Se_t)	0.0036	-	$T/{}^1d_{Se_t}^{Tl^{III}}/{}^1t_{Se_b}^{Tl^{III}}/{}^1d_{Se_{b'}}^{Tl^{III}}/{}^3d_{Se_{b'}}^{Tl^{III}}$
0	1	5	"	0.0030		
0	0	5	"	0.0006		
0	2	5	(Se_b, $2Se_{b'}$, $2Se_t$)	0.0036	-	$T/{}^1d_{Se_t}^{Tl^{III}}/{}^1d_{Se_b}^{Tl^{III}}/{}^1d_{Se_{b'}}^{Tl^{III}}/{}^3d_{Se_t}^{Tl^{III}}/{}^3d_{Se_{b'}}^{Tl^{III}}$
0	1	5	"	0.0030		
0	0	5	"	0.0006		
0	2	5	($2Se_b$, $Se_{b'}$, $2Se_t$)	0.0036	-	$T/{}^1d_{Se_t}^{Tl^{III}}/{}^1t_{Se_{b'}}^{Tl^{III}}/{}^1d_{Se_{b'}}^{Tl^{III}}/{}^3d_{Se_t}^{Tl^{III}}/$
0	1	5	"	0.0030		
0	0	5	"	0.0006		

$^{205}Tl_x^{III}\,^{203}Tl_{2-x}^{III}\,^{205}Tl_y^{I}\,^{203}Tl_{2-y}^{I}$ $^{77}Se_z\,^{0}Se_{6-z}^{4-\,a}$				isotopomer fractional abundance,[b]	multiplicity observed for the components of the subspectra in the Tl^{I} Region	
x	y	z	^{77}Se environments		^{205}Tl	^{203}Tl
2	2	5	(Se_b, $2Se_{b'}$, $2Se_t$)	0.0207	$T/{}^1d_{Se_b}^{Tl^{I}}/{}^1t_{Se_{b'}}^{Tl^{I}}/{}^3t_{Se_t}^{Tl^{I}}$	-
1	2	5	"	0.0174		
0	2	5	"	0.0036		
2	2	5	($2Se_b$, $Se_{b'}$, $2Se_t$)	0.0207	$T/{}^1d_{Se_b}^{Tl^{I}}/{}^1d_{Se_{b'}}^{Tl^{I}}/{}^3t_{Se_t}^{Tl^{I}}/{}^3d_{Se_b}^{Tl^{I}}$	-
1	2	5	"	0.0174		
0	2	5	"	0.0036		
2	1	6	($2Se_b$, $2Se_{b'}$, $2Se_t$)	0.1463	$T/{}^2d_{Tl^{I}}^{Tl^{I}}/{}^1d_{Se_b}^{Tl^{I}}/{}^1t_{Se_b}^{Tl^{I}}/{}^3t_{Se_t}^{Tl^{I}}/{}^3d_{Se_b}^{Tl^{I}}$	$T/{}^2d_{Tl^{I}}^{Tl^{I}}/{}^1d_{Se_b}^{Tl^{I}}/{}^1t_{Se_{b'}}^{Tl^{I}}/{}^3t_{Se_t}^{Tl^{I}}/{}^3d_{Se_{b'}}^{Tl^{I}}$
1	1	6	"	0.1224		
0	1	6	"	0.0256		
2	1	5	($2Se_b$, $2Se_{b'}$, Se_t)	0.0174	$T/{}^2d_{Tl^{I}}^{Tl^{I}}/{}^1d_{Se_b}^{Tl^{I}}/{}^1t_{Se_{b'}}^{Tl^{I}}/{}^3d_{Se_t}^{Tl^{I}}/{}^3d_{Se_b}^{Tl^{I}}$	$T/{}^2d_{Tl^{I}}^{Tl^{I}}/{}^1d_{Se_b}^{Tl^{I}}/{}^1t_{Se_{b'}}^{Tl^{I}}/{}^3d_{Se_t}^{Tl^{I}}/{}^3d_{Se_b}^{Tl^{I}}$
1	1	5	"	0.0145		
0	1	5	"	0.0030		
2	1	5	(Se_b, $2Se_{b'}$, $2Se_t$)	0.0087	$T/{}^2d_{Tl^{I}}^{Tl^{I}}/{}^1d_{Se_b}^{Tl^{I}}/{}^1t_{Se_{b'}}^{Tl^{I}}/{}^3t_{Se_t}^{Tl^{I}}$	$T/{}^2d_{Tl^{I}}^{Tl^{I}}/{}^1d_{Se_b}^{Tl^{I}}/{}^1t_{Se_{b'}}^{Tl^{I}}/{}^3t_{Se_t}^{Tl^{I}}$
1	1	5	"	0.0073		
0	1	5	"	0.0015		
2	1	5	(Se_b, $2Se_{b'}$, $2Se_t$)	0.0087	$T/{}^2d_{Tl^{I}}^{Tl^{I}}/{}^1t_{Se_{b'}}^{Tl^{I}}/{}^3t_{Se_t}^{Tl^{I}}/{}^3d_{Se_b}^{Tl^{I}}$	$T/{}^2d_{Tl^{I}}^{Tl^{I}}/{}^1t_{Se_{b'}}^{Tl^{I}}/{}^3t_{Se_t}^{Tl^{I}}/{}^3d_{Se_b}^{Tl^{I}}$
1	1	5	"	0.0073		
0	1	5	"	0.0015		
2	1	5	($2Se_b$, $Se_{b'}$, $2Se_t$)	0.0174	$T/{}^2d_{Tl^{I}}^{Tl^{I}}/{}^1d_{Se_b}^{Tl^{I}}/{}^1d_{Se_{b'}}^{Tl^{I}}/{}^3t_{Se_t}^{Tl^{I}}/{}^3d_{Se_b}^{Tl^{I}}$	$T/{}^2d_{Tl^{I}}^{Tl^{I}}/{}^1d_{Se_b}^{Tl^{I}}/{}^1d_{Se_{b'}}^{Tl^{I}}/{}^3t_{Se_t}^{Tl^{I}}/{}^3d_{Se_b}^{Tl^{I}}$
1	1	5	"	0.0145		
0	1	5	"	0.0030		
2	0	6	($2Se_b$, $2Se_{b'}$, $2Se_t$)	0.0306	-	$T/{}^1d_{Se_b}^{Tl^{I}}/{}^1t_{Se_{b'}}^{Tl^{I}}/{}^3t_{Se_t}^{Tl^{I}}/{}^3d_{Se_b}^{Tl^{I}}$
1	0	6	"	0.0256		
0	0	6	"	0.0054		
2	0	5	($2Se_b$, $2Se_{b'}$, Se_t)	0.0036	-	$T/{}^1d_{Se_b}^{Tl^{I}}/{}^1t_{Se_{b'}}^{Tl^{I}}/{}^3d_{Se_t}^{Tl^{I}}/{}^3d_{Se_b}^{Tl^{I}}$
1	0	5	"	0.0030		
0	0	5	"	0.0006		
2	0	5	(Se_b, $2Se_{b'}$, $2Se_t$)	0.0036	-	$T/{}^1d_{Se_b}^{Tl^{I}}/{}^1t_{Se_{b'}}^{Tl^{I}}/{}^3t_{Se_t}^{Tl^{I}}$
1	0	5	"	0.0030		
0	0	5	"	0.0006		
2	0	5	($2Se_b$, $Se_{b'}$, $2Se_t$)	0.0036	-	$T/{}^1d_{Se_b}^{Tl^{I}}/{}^1d_{Se_{b'}}^{Tl^{I}}/{}^3t_{Se_t}^{Tl^{I}}/{}^3d_{Se_b}^{Tl^{I}}$
1	0	5	"	0.0030		
0	0	5	"	0.0006		

[*] For footnotes a-c see footnotes to Table 4.

^{203}Tl interenvironmental (2390−6456 Hz) and ^{205}Tl−^{203}Tl intraenvironmental couplings (1312−4536 Hz). Descriptions of the most important contributing isotopomers and their most prominent spectral features are provided and discussed below. Symbols used in the following discussion are defined in footnote c of Table 4.

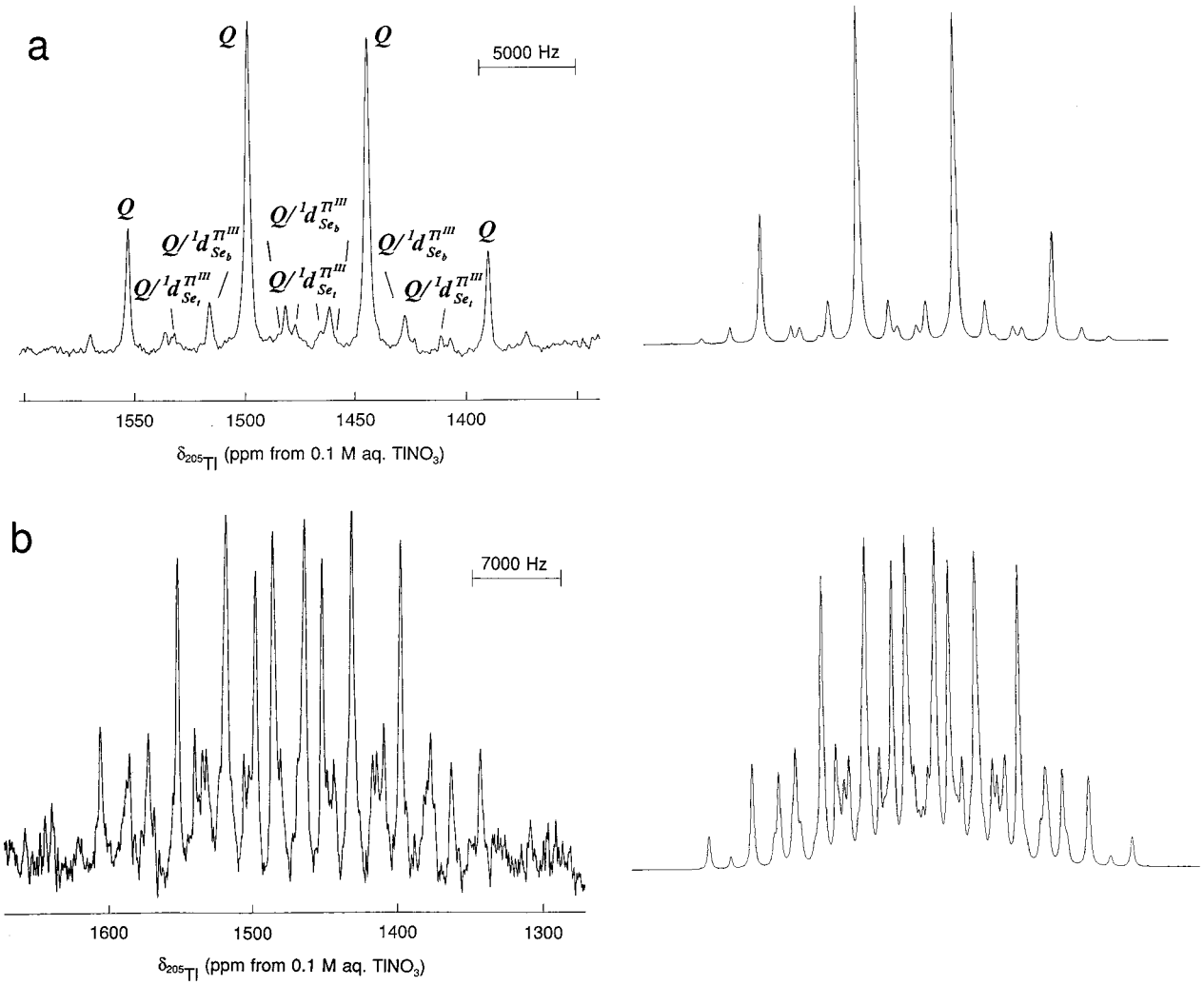

Figure 4. ^{205}Tl (115.444 MHz) NMR spectra of the Tl^{III} environment in the $Tl_4Se_5^{4-}$ anion recorded in liquid NH_3 at −70 °C for (a) natural abundance and (b) 94.4% ^{77}Se-enriched samples. For clarity, only the subspectra associated with the two central lines of the quartet (Q) are labeled in (a). Simulated spectra are the right-hand traces and peak labels are defined in Table 4.

1. $Tl_4Se_5^{4-}$. The ^{205}Tl NMR spectrum of the $Tl_4Se_5^{4-}$ anion in liquid NH_3 at −70 °C comprises two resonances, a quartet and a doublet, respectively, in the Tl^{III} and Tl^{I} regions. The more intense Tl^{III} quartet (Q) (1472 ppm; Figure 4) arises from the $^{205}Tl^{III}\,^{205}Tl_x^{I}\,^{203}Tl_{3-x}^{I}\,^{0}Se_5$ ($x = 0-3$) isotopomeric subspectra and an interenvironmental coupling between the observed Tl^{III} environment and three Tl^{I} atoms, $^2J(^{205}Tl^{III}-^{205(3)}Tl^{I}) = 6279$ Hz. Satellite doublet subspectra symmetrically disposed about each component of the quartet, $Q/^1d^{Tl^{III}}_{Se_b}$ and $Q/^1d^{Tl^{III}}_{Se_t}$, were also observed and result from $^1J(^{205}Tl^{III}-^{77}Se_b) = 3958$ Hz and $^1J(^{205}Tl^{III}-^{77}Se_t) = 7645$ Hz of the respective isotopomers $^{205}Tl^{III}\,^{205}Tl_x^{I}\,^{203}Tl_{3-x}^{I}\,^{77}Se_b\,^{0}S_4$ ($Q/^1d^{Tl^{III}}_{Se_b}$) and $^{205}Tl^{III}\,^{205}Tl_x^{I}\,^{203}Tl_{3-x}^{I}\,^{77}Se_t\,^{0}Se_4$ ($Q/^1d^{Tl^{III}}_{Se_t}$). The I_s/I_c ratios are consistent with three Se_b atoms and one Se_t atom (structure **I**).

The most intense feature in the Tl^{I} region of the ^{205}Tl spectrum is a doublet (D) (5531 ppm; Figure 5) arising from an interenvironmental coupling between one Tl^{I} and one Tl^{III} atom, $^2J(^{205}Tl^{I}-^{205(3)}Tl^{III}) = 6272$ Hz, of the isotopomers, $^{205}Tl^{III}\,^{205}Tl_3^{I}\,^{0}Se_5$ and $^{203}Tl^{III}\,^{205}Tl_3^{I}\,^{0}Se_5$. Each of the doublet (D) components is flanked by doublet ^{203}Tl satellite subspectra ($D/^2d^{Tl^{I}}_{Tl^{I}}$) assigned to the $^{205}Tl^{III}\,^{205}Tl_2^{I}\,^{203}Tl^{I}\,^{0}Se_5$ and the $^{203}Tl^{III}\,^{205}Tl_2^{I}\,^{203}Tl^{I}\,^{0}Se_5$ isotopomers, which arise from the intraenvironmental coupling, $^2J(^{205}Tl^{I}-^{203}Tl^{I}) = 2549$ Hz. The I_s/I_c ratios indicate that each Tl^{I} nucleus is spin-coupled to two other Tl^{I} nuclei. The third major feature is a triplet ($D/^2t^{Tl^{I}}_{Tl^{I}}$), whose central transition overlaps with the main doublet, arising from the $^{205}Tl^{I}\,^{205}Tl^{I}\,^{203}Tl_2^{I}\,^{0}Se_5$ and $^{203}Tl^{I}\,^{205}Tl^{I}\,^{203}Tl_2^{I}\,^{0}Se_5$ isotopomers. The corresponding $^2J(^{203}Tl^{I}-^{205(3)}Tl^{III}) = 6227$ Hz interenvironmental coupling, associated with the $^{203}Tl^{III}\,^{205}Tl_x^{I}\,^{203}Tl_{3-x}^{I}\,^{0}Se_5$ isotopomer, was determined by recording the ^{203}Tl NMR spectrum in which the ^{205}Tl satellite intensities are enhanced when compared with the ^{203}Tl satellites in the ^{205}Tl NMR spectrum owing to the over 2-fold greater natural abundance of the ^{205}Tl nuclide (Figure 5c). The observed ratio, $^2J(^{205}Tl-^{205(3)}Tl)/^2J(^{203}Tl-^{205(3)}Tl) = 1.008$ (R_J), is in good agreement with the ratio of the gyromagnetic ratios of the ^{205}Tl to ^{203}Tl nuclides, $\gamma(^{205}Tl)/\gamma(^{203}Tl) = 1.010$.[27] The broader line widths associated with the Tl^{I} resonance are attributed to the presence of unresolved ^{77}Se satellites. The corresponding $^1J(^{77}Se_{b'}-^{205(3)}Tl^{I}) = 600$ Hz, $^1J(^{77}Se_b-^{205(3)}Tl^{I}) = 240$ Hz, $^3J(^{77}Se_b-^{205(3)}Tl^{I}) = 150$ Hz, and $^3J(^{77}Se_t-^{205(3)}Tl^{I}) = 70$ Hz couplings were obtained from the ^{77}Se NMR spectrum and from the ^{205}Tl spectrum of a ^{77}Se-enriched sample.

The determination of the isotopomeric subspectra contributing to the ^{203}Tl and ^{205}Tl spectra of the 94.4% ^{77}Se-enriched $Tl_4Se_5^{4-}$ anion (hereafter denoted as $Tl_4{}^{77}Se_5^{4-}$) is based on the natural

(27) Mason, J. In *Multinuclear NMR*; Mason, J., Ed.; Plenum Press: New York, 1987; Appendix, pp 623−629.

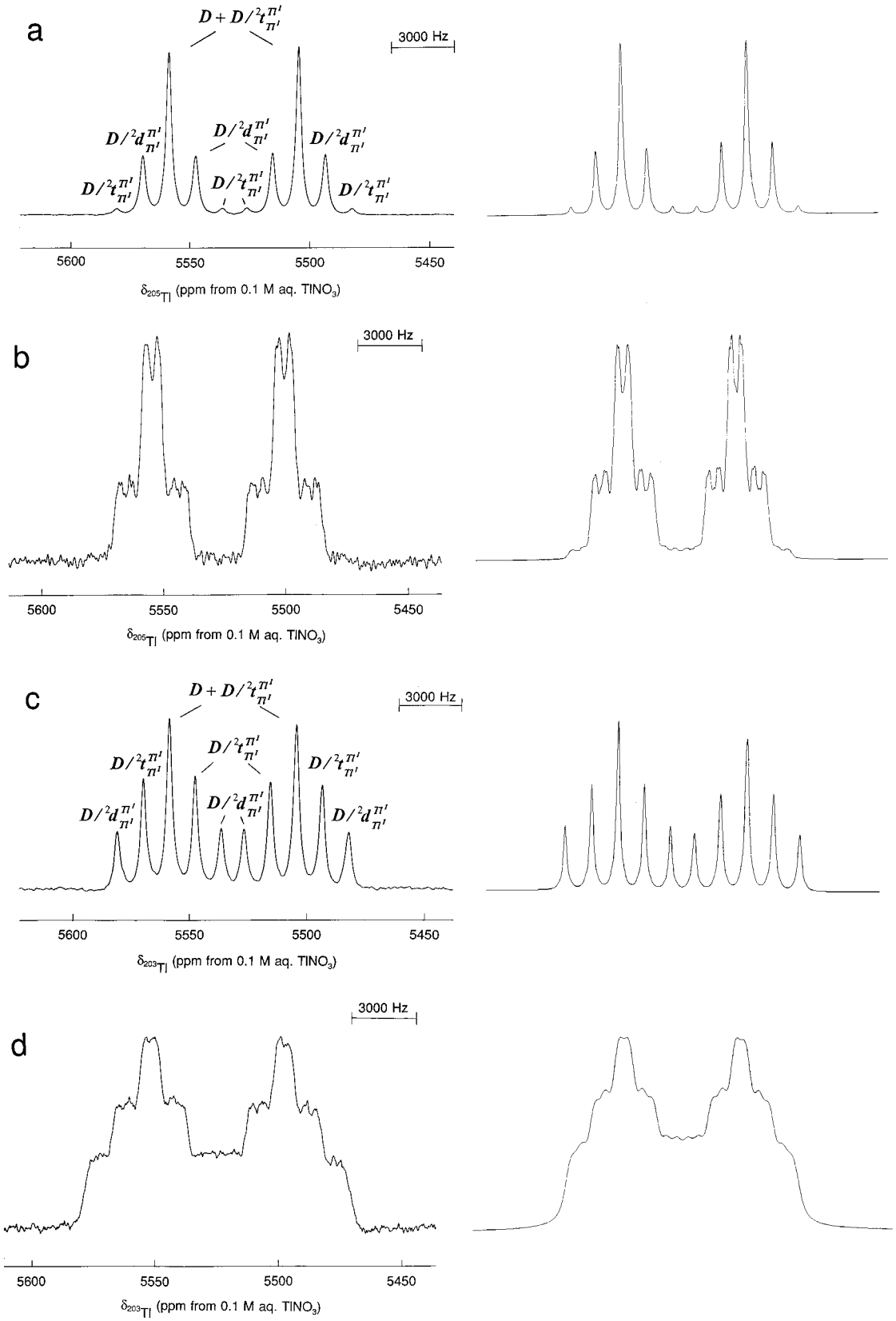

Figure 5. (a,b) ^{205}Tl (115.444 MHz) and (c,d) ^{203}Tl (114.319 MHz) NMR spectra of the Tl^{III} environment in the $Tl_4Se_5^{4-}$ anion recorded in liquid NH_3 at −70 °C for (a,c) natural abundance and (b,d) 94.4% ^{77}Se-enriched samples. Simulated spectra are the right-hand traces, and peak labels are defined in Table 4.

abundance assignments. The increase in spectral complexity (Table 4) primarily results from multiplets $Q/^1d^{Tl^{III}}_{Se_t}/^1q^{Tl^{III}}_{Se_b}/^1d^{Tl^{III}}_{Se_{b'}}$ and $D/^1d^{Tl^{I}}_{Se_{b'}}/^1t^{Tl^{I}}_{Se_b}/^3d^{Tl^{I}}_{Se_b}/^3d^{Tl^{I}}_{Se_t}$, which comprise the most intense features in the Tl^{III} and Tl^{I} regions, respectively. Successful simulation of the enriched spectra (Figures 4 and 5) confirmed all prior assignments of the natural abundance spectra.

The ^{77}Se NMR spectrum of the $Tl_4{}^{77}Se_5^{4-}$ anion at −70 °C (Figure 6) consists of three resonances having relative intensities

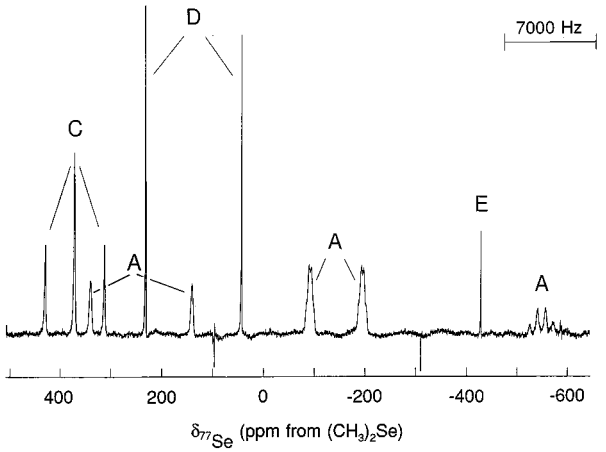

Figure 6. ^{77}Se (38.168 MHz) NMR spectrum of the ^{77}Se-enriched (A) $Tl_4Se_5^{4-}$, (C) $Tl_2Se_2^{2-}$, (D) $TlSe_3^{3-}$, and (E) Se^{2-} anions recorded in liquid NH_3 at −70 °C.

of 1:3:1, in agreement with the respective number of Se_t, Se_b, and $Se_{b'}$ atoms. The signal at −548 ppm consists of a quartet [$^1J(^{77}Se_{b'}-^{205(3)}Tl^I) = 600$ Hz] of doublets [$^3J(^{77}Se_{b'}-^{205(3)}Tl^{III}) \approx 100$ Hz] and is attributed to $Se_{b'}$. The signal at 250 ppm is a doublet [$^1J(^{77}Se_t-^{205(3)}Tl^{III}) = 7537$ Hz] of quartets [$^3J(^{77}Se_t-^{205(3)}Tl^I) \approx 150$ Hz] and is assigned to Se_t. The resonance assigned to Se_b appears at −143 ppm and consists of a doublet-of-triplets-of-doublets arising from $^1J(^{77}Se_b-^{205(3)}Tl^{III}) = 3928$ Hz (doublet), $^1J(^{77}Se_b-^{205(3)}Tl^I) = 240$ Hz (triplet), and $^3J(^{77}Se_b-^{205(3)}Tl^I) \approx 70$ Hz (doublet). The ^{77}Se resonances were assigned by comparison with the $J(^{77}Se-^{205(3)}Tl)$ couplings observed in the $^{205(3)}$Tl spectra.

The multiplet patterns and I_s/I_c ratios are consistent with a $Tl_4Se_5^{4-}$ anion containing three Tl^I atoms and one Tl^{III} atom in which Tl^{III} is bonded to one terminal (Se_t) and three bridging (Se_b) selenium atoms and in which the three Tl^I atoms are bonded to the bridging Se_b atoms and to a unique bridging selenium atom ($Se_{b'}$). The Tl and bridging Se atoms form a Tl_4Se_4 cube with the Tl^{III} atom bonded to a unique exo-Se_t atom (structure I).

2. $Tl_4Se_6^{4-}$. The ^{205}Tl NMR spectrum of the $Tl_4Se_6^{4-}$ anion in the liquid NH_3 extract at −20 °C (Figure 7a,b) consists of two triplets in the Tl^{III} and Tl^I regions. The most intense feature in the Tl^{III} region is a triplet (T) (1680 ppm) arising from an interenvironmental coupling between one Tl^{III} and two Tl^I atoms of the isotopomers $^{205}Tl_2^{III}\,^{205}Tl_y^I\,^{203}Tl_{2-y}^I\,^0Se_6$ ($x = 0-2$), where $^2J(^{205}Tl^{III}-^{205(3)}Tl^I) = 3738$ Hz. Each of the triplet components is flanked by doublet ^{203}Tl satellite subspectra ($T/^2d_{Tl^{III}}^{Tl^{III}}$) assigned to $^{205}Tl^{III}\,^{203}Tl^{III}\,^{205}Tl_y^I\,^{203}Tl_{2-y}^I\,^0Se_6$ ($x = 0-2$), which arise from the intraenvironmental coupling $^2J(^{205}Tl^{III}-^{203}Tl^{III}) = 1538$ Hz. The I_s/I_c ratios indicate that each Tl^{III} nucleus is spin-coupled to an additional Tl^{III} nucleus. Satellite doublet subspectra $T/^1d_{Se_b}^{Tl^{III}}$, $T/^1d_{Se_{b'}}^{Tl^{III}}$, and $T/^1d_{Se_t}^{Tl^{III}}$, symmetrically disposed about each component of the triplet, were also observed and result from $^1J(^{205}Tl^{III}-^{77}Se_b) = 3050$ Hz, $^1J(^{205}Tl^{III}-^{77}Se_{b'}) = 4254$ Hz, and $^1J(^{205}Tl^{III}-^{77}Se_t) = 8735$ Hz of their respective isotopomers $^{205}Tl_2^{III}\,^{205}Tl_y^I\,^{203}Tl_{2-y}^I\,^{77}Se_b\,^0Se_6$ ($T/^1d_{Se_b}^{Tl^{III}}$), $^{205}Tl_2^{III}\,^{205}Tl_y^I\,^{203}Tl_{2-y}^I\,^{77}Se_{b'}\,^0Se_6$ ($T/^1d_{Se_{b'}}^{Tl^{III}}$), and $^{205}Tl_2^{III}\,^{205}Tl_y^I\,^{203}Tl_{2-y}^I\,^{77}Se_t\,^0Se_6$ ($T/^1d_{Se_t}^{Tl^{III}}$) ($y = 0-2$). The long-range $^3J(^{205}Tl^{III}-^{77}Se_{b'}) \approx 50$ Hz coupling was estimated from the ^{77}Se NMR spectrum. The I_s/I_c ratios are consistent with two Se_b, one $Se_{b'}$, and one Se_t atoms, respectively (structure **II**). The $^2J(^{203}Tl^{III}-^{205(3)}Tl^I) = 3683$ Hz interenvironmental coupling associated with the $^{203}Tl_2^{III}\,^{205}Tl_y^I\,^{203}Tl_{2-y}^I\,^0Se_6$ ($y = 0-2$) isotopomer was determined by recording the ^{203}Tl NMR spectrum (Figure 7c) and confirmed by the $^2J(^{205}Tl-^{205(3)}Tl)/^2J(^{203}Tl-^{205(3)}Tl) = 1.014$ ratio.

The most intense feature in the Tl^I region of the ^{205}Tl spectrum is also a triplet (T) (5433 ppm; Figure 8a) arising from the same interenvironmental coupling between one Tl^I and two Tl^{III} atoms, $^2J(^{205}Tl^I-^{205(3)}Tl^{III}) = 3721$ Hz, of the isotopomers $^{205}Tl_x^{III}\,^{203}Tl_{x-2}^{III}\,^{205}Tl_2^I\,^0Se_6$ ($x = 0-2$). Each of the triplet (T) components is flanked by doublet ^{203}Tl satellite subspectra ($T/^2d_{Tl^I}^{Tl^I}$) that are assigned to $^{205}Tl_x^{III}\,^{203}Tl_{x-2}^{III}\,^{205}Tl^I\,^{203}Tl^I\,^0Se_6$ ($x = 0-2$) and arise from $^2J(^{205}Tl^I-^{203}Tl^I) = 4536$ Hz. The I_s/I_c ratios indicate that each Tl^I nucleus is spin-coupled to one other Tl^I nucleus. The assignment was confirmed by recording the ^{203}Tl spectrum ($R_J = 1.012$) (Figure 8c). As observed in the −70 °C spectrum, the broader line widths associated with the Tl^I resonance are attributed to unresolved ^{77}Se satellites arising from $^1J(^{205}Tl^I-^{77}Se_{b'}) \approx 400$ Hz, $^1J(^{205}Tl^I-^{77}Se_b) \approx 600$ Hz, $^3J(^{205}Tl^I-^{77}Se_t) \approx 150$ Hz, and $^3J(^{205}Tl^I-^{77}Se_b) \approx 50$ Hz, which were estimated from the ^{205}Tl and ^{77}Se NMR spectra of the ^{77}Se-enriched $Tl_4{}^{77}Se_6^{4-}$ anion (hereafter denoted as $Tl_4{}^{77}Se_6^{4-}$). Successful simulation of the ^{205}Tl NMR spectra of the $Tl_4{}^{77}Se_6^{4-}$ anion (Figures 7b and 8b) confirmed all assignments.

The ^{77}Se NMR spectrum of the $Tl_4{}^{77}Se_6^{4-}$ anion at −20 °C (Figure 9) consists of three resonances in an approximate 1:1:1 ratio, which is in agreement with the respective number of Se_t, Se_b, and $Se_{b'}$ atoms. However, they are not as well resolved as those observed at −70 °C so that smaller ^3J couplings could only be estimated from the line widths of the signals. The multiplets assigned to $Se_{b'}$, Se_t, and Se_b result from Se−Tl spin−spin couplings and are complex: $Se_{b'}$ (−88 ppm) arises from $^1J(^{77}Se_{b'}-^{205(3)}Tl^{III}) = 4254$ Hz (doublet), $^1J(^{77}Se_{b'}-^{205(3)}Tl^I) \approx 400$ Hz (triplet), and $^3J(^{77}Se_{b'}-^{205(3)}Tl^{III}) \approx 50$ Hz (doublet); Se_t (272 ppm) arises from $^1J(^{77}Se_t-^{205(3)}Tl^{III}) = 8735$ Hz (doublet), $^3J(^{77}Se_t-^{205(3)}Tl^{III})$ (unresolved doublet), and $^3J(^{77}Se_t-^{205(3)}Tl^I) \approx 150$ Hz (triplet); Se_b (364 ppm) arises from $^1J(^{77}Se_b-^{205(3)}Tl^{III}) = 3050$ Hz (triplet), $^1J(^{77}Se_b-^{205(3)}Tl^I) \approx 600$ Hz (doublet), and $^3J(^{77}Se_b-^{205(3)}Tl^I) \approx 70$ Hz (doublet). The resonances were assigned by comparing the $J(^{77}Se-^{205(3)}Tl)$ couplings observed in the ^{77}Se spectrum with those obtained from the ^{205,203}Tl spectra.

The multiplet patterns and I_s/I_c ratios are consistent with a $Tl_4Se_6^{4-}$ anion containing two Tl^{III} atoms, each bonded to one terminal (Se_t) and three bridging (two Se_b and one $Se_{b'}$) selenium atoms, and two Tl^I atoms bonded to one Se_b and two $Se_{b'}$ atoms. The Tl and bridging Se atoms form a Tl_4Se_4 cube in which each Tl^{III} atom is bonded to an *exo*-Se_t atom.

3. $Tl_3Se_x^{y-}$. In addition to resonances associated with the $Tl_4Se_5^{4-}$ and $Tl_4Se_6^{4-}$ anions, the ^{205}Tl NMR spectrum in en at 0 °C (Figure 10) contains a new doublet and a new triplet pattern in the Tl^{III} and Tl^I regions, respectively. The doublet (1876 ppm; Figure 10a) arises from an interenvironmental coupling between the Tl^{III} environment and one Tl^I atom, $^2J(^{205}Tl^I-^{205(3)}Tl^{III}) = 3576$ Hz. Each of the components of the doublet is flanked by doublet ^{203}Tl satellites assigned to the intraenvironmental coupling, $^2J(^{205}Tl^{III}-^{203}Tl^{III}) = 1312$ Hz. The triplet (5258 ppm; Figure 10b) is assigned to Tl^I and arises from an interenvironmental coupling with two chemically equivalent Tl^{III} atoms, $^2J(^{205}Tl^{III}-^{205(3)}Tl^I) = 3628$ Hz. Although Tl−Se coupling could not be observed, the preliminary data indicate that this anion contains two Tl^{III} and one Tl^I atom and can be formulated as the $Tl_3Se_x^{y-}$ anion.

Chemical Shifts and Coupling Constants. The $^{205/203}$Tl chemical shifts for the $Tl_4Se_5^{4-}$ and $Tl_4Se_6^{4-}$ anions exhibit the same trend as those of the mixed chalcogen Tl^{III} and Tl^I anions,

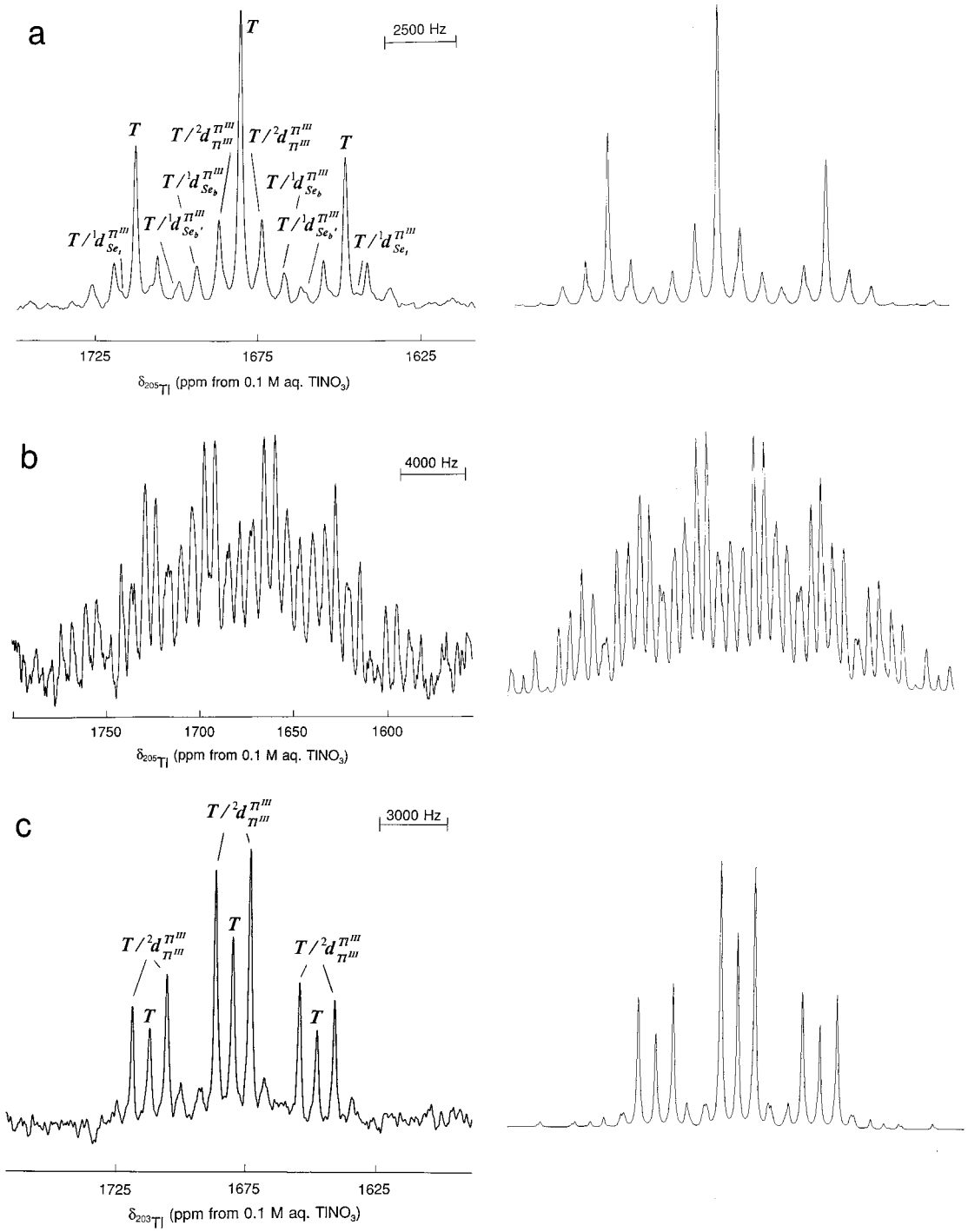

Figure 7. (a,b) ^{205}Tl (115.444 MHz) and (c) ^{203}Tl (114.319 MHz) NMR spectra of the Tl^{III} environment in the $Tl_4Se_6^{4-}$ anion recorded in liquid NH_3 at −20 °C for (a,c) natural abundance and (b) 94.4% ^{77}Se-enriched samples. For clarity, only the subspectra associated with the central line of the triplet (T) have been labeled. Simulated spectra are the right-hand traces, and peak labels are defined in Table 4.

$TlCh_3^{3-}$ [8] and $Tl_2Ch_2^{2-}$ [2,8] (Ch = Se, Te), with the thallium resonances of the Tl^{III} anions being considerably more shielded than those of the Tl^{I} anions. The chemical shifts of the $Tl_2^{I}Se_2^{2-}$ and $Tl^{III}Se_3^{3-}$ anions are very similar to those of thalliums having the same oxidation states in $Tl_4Se_5^{4-}$ and $Tl_4Se_6^{4-}$ and further substantiate the trend toward higher shielding with increased coordination number that has been observed for other main group elements.[28] The trend is also the reverse of the calculated atomic charges (Table 6), which are significantly higher for Tl^{III} than for Tl^{I} in $Tl_4Se_5^{4-}$ and $Tl_4Se_6^{4-}$. It is also interesting to note that the chemical shifts of the Tl^{I} atoms in both anions (5110−5600 ppm) are significantly more deshielded compared with those of the structurally related neutral tetrameric alkoxides, $(TlOR)_4$ (2580−3183 ppm),[29] despite their negative anionic charges and the lower electronegativity of selenium. The extreme high-frequency ^{207}Pb, ^{205}Tl, and ^{119}Sn chemical shifts of $Pb_2Se_xTe_{3-x}^{2-}$,[16] Ph_3Pb^{3-},[30] $Pb[N(SiMe_3)_2]_2$,[31] $M_2Ch_3^{2-}$,[17] and $TlMTe_3^{3-}$ [17] (M = Sn, Pb; Ch = Se or Te) have been

(28) Mason, J. In *Multinuclear NMR*; Mason, J., Ed.; Plenum Press: New York, 1987; Chapter 3, pp 66−67.

(29) Hinton, J. F.; Briggs, R. W. In *NMR and the Periodic Table*; Harris, R. K., Mann, B. E., Eds.; Academic Press Inc.: London, 1978; Chapter 9, pp 279−308.

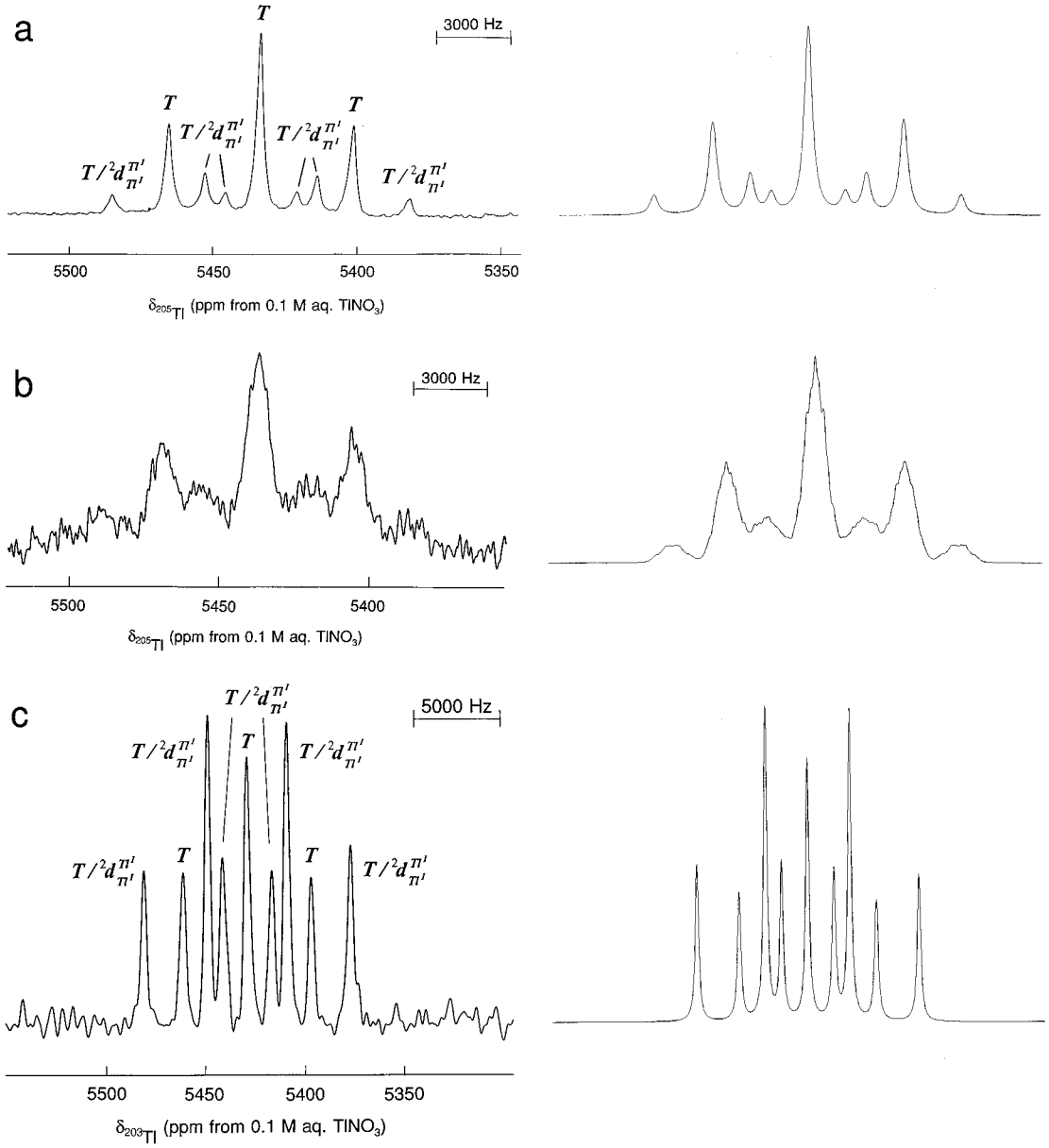

Figure 8. (a,b) ^{205}Tl (115.444 MHz) and (c) ^{203}Tl (114.319 MHz) NMR spectra of the Tl^{I} environment in the $Tl_4Se_6^{4-}$ anion recorded in liquid NH_3 at −20 °C for (a,c) natural abundance and (b) 94.4% ^{77}Se-enriched samples. Simulated spectra are the right-hand traces, and peak labels are defined in Table 4.

attributed to spin−orbit induced changes in the wave function[17,30] and termed the "heavy-atom shift of a heavy atom" (HAHA) effect,[30] which are likely responsible for very large paramagnetic contributions to the shielding of the heavy atom. The effect is likely an important contributor to the paramagnetic terms of Tl^{I} in $Tl_4Se_5^{4-}$ and $Tl_4Se_6^{4-}$, which, like the prior examples, have a lone valence electron pair at the heavy main group metal.

All ^{77}Se resonances in the $Tl_4Se_6^{4-}$ anion are deshielded with respect to those of $Tl_4Se_5^{4-}$. As expected, the Se_t chemical shift in $Tl_4Se_6^{4-}$ (272 ppm) is very similar to that in $Tl_4Se_5^{4-}$ (250 ppm) because the immediate directly bonded environments of the Se_t atoms are the same in both anions, and indeed, these atoms are shown to have similar atomic charges and total bond valencies (Table 6). These terminal selenium chemical shifts are more deshielded than those of the trigonal planar $Tl^{III}Se_3^{3-}$

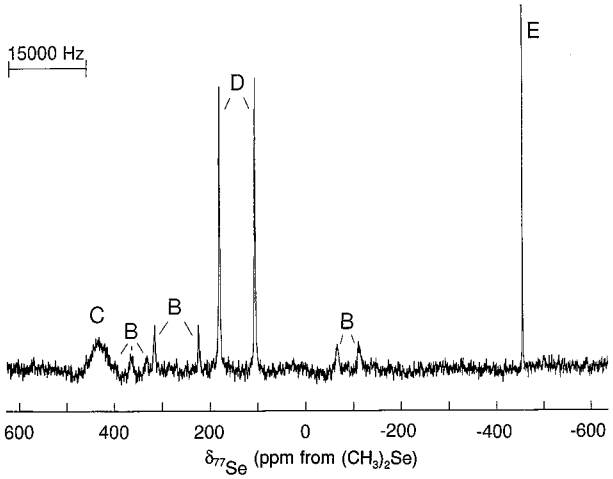

Figure 9. ^{77}Se (38.168 MHz) NMR spectrum of the ^{77}Se-enriched (B) $Tl_4Se_6^{4-}$, (C) $Tl_2Se_2^{2-}$, (D) $TlSe_3^{3-}$, and (E) Se^{2-} anions recorded in liquid NH_3 at −20 °C.

(30) Edlund, U.; Lejon, T.; Pyykkö, P.; Venkatachalam, T. K.; Buncel, E. *J. Am. Chem. Soc.* **1987**, *109*, 5982.

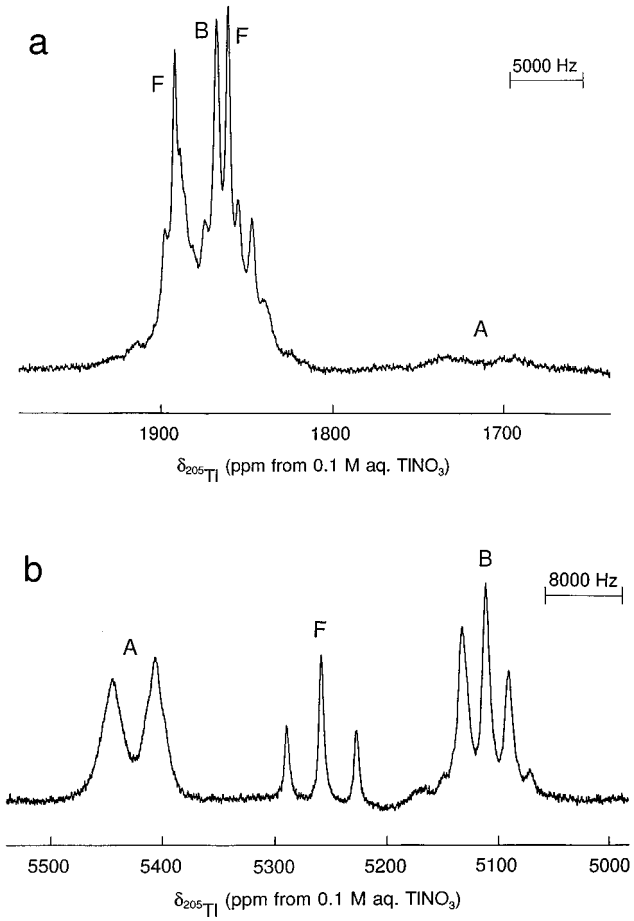

Figure 10. ^{205}Tl (115.444 MHz) NMR spectra of the (a) Tl(I) and (b) Tl(III) environments in the (A) $Tl_4Se_5^{4-}$, (B) $Tl_4Se_6^{4-}$, and (F) $Tl_3Se_x^{y-}$ anions recorded in en at 0 °C.

anion (136−140 ppm),[8] suggesting that more of the anion charge is localized on the terminal selenium atoms. The chemical shift of $Se_{b'}$ in $Tl_4Se_6^{4-}$ (−88 ppm) is comparable with that of Se_b in $Tl_4Se_5^{4-}$ (−143 ppm), in accord with both seleniums having the same connectivities to two Tl^I atoms and one Tl^{III} atom and similar atomic charges (Table 6). The $Se_{b'}$ environments of $Tl_4Se_5^{4-}$ and $Tl_4Se_6^{4-}$ are presumably more shielded than the Se_b environments because the terminal seleniums bonded to Tl^{III} delocalize charge onto the metal atom by means of a multiple bonding interaction (see Computational Results). The Tl^{III} atoms maintain their valency requirements by, in turn, localizing negative charge onto the directly bonded bridging seleniums (Se_b and $Se_{b'}$). These charge localizations are greater for $Se_{b'}$ than for Se_b in both anions (Table 6) because Se_b and $Se_{b'}$ are differentiated on the basis of the greater number of bonds they form with Tl^I ($Se_{b'}$) and with Tl^{III} (Se_b), and this leads to deshielding of Se_b relative to $Se_{b'}$. The large decreases in the ^{77}Se shieldings of $Se_{b'}$ and Se_b of approximately 460 and 510 ppm, respectively, on going from $Tl_4Se_5^{4-}$ to $Tl_4Se_6^{4-}$ are also a reflection of the greater charge localization onto the selenium bridges that is expected when the numbers of Tl^{III} centers and terminal seleniums are doubled, and this is confirmed by their relative atomic charges (Table 6).

The $^2J(Tl^{III}-Tl^{III})$ and $^2J(Tl^I-Tl^{III})$ couplings reported in this work are the first $Tl^{I/III}-Tl^{III}$ couplings to be reported. The only other Tl−Tl couplings to have been reported are for Tl^I in $Tl_2Ch_2^{2-}$ (Se, 3602−3995 Hz; Te, 6328−7591 Hz; Se/Te, 1945−2800 Hz)[2,8] and for the Tl^I alkoxide tetramers, $(TlOR)_4$ (2170−2769 Hz).[29] The $^2J(Tl^I-Tl^I)$ couplings in this study are similar to those reported for the related $Tl_2Se_2^{2-}$ anion. It is noteworthy that the $^2J(Tl^I-Tl^I)$ coupling observed in the $Tl_4Se_5^{4-}$ anion (2508−2549 Hz) is very similar to those observed for the related oxo-bridged $(TlOR)_4$ cubes.

The trend $^2J(Tl^I-Tl^I) > {}^2J(Tl^I-Tl^{III}) > {}^2J(Tl^{III}-Tl^{III})$ in $Tl_4Se_6^{4-}$ follows the valence s orbital populations on the coupled centers and is in qualitative agreement with the formalism for the Fermi contact contribution to the *J* coupling, which is proportional to the product of the s electron densities on the coupled centers.[32,33] In the case of $Tl_4Se_5^{4-}$, the trend $^2J(Tl^I-Tl^I) < {}^2J(Tl^I-Tl^{III})$ is reversed and may be largely attributed to the greater number of $^2J(Tl^I-Tl^{III})$ coupling paths that are available in this anion. Unlike the Tl−Tl couplings of the $Tl_2Ch_2^{2-}$ anions, the Tl−Tl couplings of $Tl_4Se_5^{4-}$ and $Tl_4Se_6^{4-}$ anions vary slightly (ca. 100 Hz) with the temperature and the nature of the solvent (Table 3) and may be a consequence of their greater rigidity when compared with the $Tl_2Ch_2^{2-}$ anions,[2] which are highly deformable in solution.

The $^1J(^{205}T^{III}-{}^{77}Se_t)$ couplings are larger than the $^1J(^{205}Tl^{I/III}-{}^{77}Se_{b,b'})$ couplings and are consistent with higher bond orders and shorter bond length for the $Tl^{III}-Se_t$ bond when compared to those of $Tl^I-Se_{b'}$ and $Tl^{III}-Se_{b'}$ bonds (see Computational Results). The trend, $^1J(^{205}Tl^{III}-{}^{77}Se_t) > {}^1J(^{205}Tl^I-{}^{77}Se_b)$ has been observed previously for $TlSe_3^{3-}$ [8] and $Tl_2Se_2^{2-}$ [2,8] where $^1J(^{205}Tl^{III}-{}^{77}Se_t)$ and $^1J(^{205}Tl^I-{}^{77}Se_b)$ were 7211−7250 and 3560−3995 Hz, respectively.

Computational Results. Geometries and Bonding in $Tl_4Se_4^{4-}$, $Tl_4Se_5^{4-}$, $Tl_4Se_6^{4-}$, and $Tl_5Se_5^{3-}$. The $Tl_4Se_5^{4-}$ and $Tl_4Se_6^{4-}$ anions are formally derived from the unknown $Tl_4Se_4^{4-}$ anion by two successive two-electron oxidation−reductions between a Tl^I center and Se^0 to give one and two exo-selenium atoms, respectively, bonded to Tl^{III}. The geometries of the anions are in accord with the topological approach of King.[34] The $Tl_4Se_4^{4-}$ anion possesses 40 valence electrons of which 16 are allocated to the 8 exoskeletal electron pairs and 24 are allocated to 12 bonding skeletal electron pairs. The valence electron counts are 46 for $Tl_4Se_5^{4-}$ and 52 for $Tl_4Se_6^{4-}$, with 12 electron pairs also allocated to bonding pairs in these anions. According to the formalism of King, the (8, 12, 6) polyhedron from which the geometries of all three anions are derived is a cube. The anions are electron-precise with respect to the 12 bonding pairs of their cores, which comprise the two-center−two-electron bonds of the cube edges.

The X-ray structure of the $Tl_5Se_5^{3-}$ anion shows that it is also derived from a cube and is closely related to the structures of the $Tl_4Se_5^{4-}$ and $Tl_4Se_6^{4-}$ anions. The $Tl_5Se_5^{3-}$ anion can be formally viewed as a Lewis acid−base interaction between the electron-precise $Tl_4Se_5^{4-}$ anion and the Tl^+ cation, resulting in an electron-precise adduct. The total number of valence electrons to consider for this system is 48. Subtraction of the 32 electrons allocated to the 2-electron bonds that form the 16 edges of the polyhedron leaves 8 exoskeletal electron pairs to be allocated as follows: Tl^I's (4 pairs), unique Se bridge to the Tl^I cap (2 pairs), three-coordinate Se's (2 pairs). The Tl^{III} and the four-coordinate Se's contribute no exoskeletal electron pairs. Interestingly, the three Tl−Se contacts of the capping Tl^I are determined from the X-ray structure (Table 2) to be identical within experimental error and are very similar to, or just slightly longer than, other Tl^I-Se distances in the cube.

1. Geometry Optimizations. (a) $Tl_4Se_4^{4-}$. Optimization was started from the cubic T_d anion at the HF level of theory. The

(31) Wrackmeyer, B. J. *Magn. Reson.* **1985**, *61*, 536.
(32) Jameson, C. J. In *Multinuclear NMR*; Mason, J., Ed.; Plenum Press: New York, 1987; Chapter 4, p 89.
(33) Pople, J. A.; Santry, D. P. *Mol. Phys.* **1964**, *8*, 1.
(34) King, R. B. *J. Am. Chem. Soc.* **1969**, *91*, 7211.

Table 6. Natural Atomic Charges, Mayer Natural Atomic Orbital Valencies, and Natural Atomic Orbital Bond Orders between Atoms at the MP2 Level in $Tl_4Se_4^{4-}$ (T_d), $Tl_4Se_5^{4-}$ (C_{3v}), $Tl_4Se_6^{4-}$ (C_{2v}), and $Tl_5Se_5^{3-}$ (C_1 and C_s)

$Tl_4Se_4^{4-}$ (T_d)

atom	Tl(1)	Se(1)	Tl(2)	Se(2)	Tl(3)	Se(3)	Tl(4)	Se(4)
charge	0.33	−1.33	0.33	−1.33	0.33	−1.33	0.33	−1.33
valency	1.21	0.87	1.21	0.87	1.21	0.87	1.21	0.87
bond orders								
Tl(1)	0.00							
Se(1)	0.32	0.00						
Tl(2)	0.09	0.32	0.00					
Se(2)	0.32	−0.03	0.32	0.00				
Tl(3)	0.09	−0.02	0.09	0.32	0.00			
Se(3)	−0.02	−0.03	0.32	−0.03	0.32	0.00		
Tl(4)	0.09	0.32	0.09	−0.02	0.09	0.32	0.00	
Se(4)	0.32	−0.03	−0.02	−0.03	0.32	−0.03	0.32	0.00

$Tl_4Se_5^{4-}$ (C_{3v})

atom	Tl(1)	Se(1)	Tl(2)	Se(2)	Tl(3)	Se(3)	Tl(4)	Se(4)	Se(5)
charge	1.03	−1.14	0.33	−1.14	0.33	−1.30	0.33	−1.14	−1.30
valency	2.58	1.02	1.25	1.02	1.25	0.91	1.25	1.02	0.67
bond orders									
Tl(1)	0.00								
Se(1)	0.52	0.00							
Tl(2)	0.08	0.33	0.00						
Se(2)	0.52	−0.05	0.33	0.00					
Tl(3)	0.08	−0.01	0.09	0.33	0.00				
Se(3)	−0.02	−0.02	0.33	−0.02	0.33	0.00			
Tl(4)	0.08	0.33	0.09	−0.01	0.09	0.33	0.00		
Se(4)	0.52	−0.05	−0.01	−0.05	0.33	−0.02	0.33	0.00	
Se(5)	0.79	−0.04	0.00	−0.04	0.00	0.00	0.00	−0.04	0.00

$Tl_4Se_6^{4-}$ (C_{2v})

atom	Tl(1)	Se(1)	Tl(2)	Se(2)	Tl(3)	Se(3)	Tl(4)	Se(4)	Se(5)	Se(6)
charge	1.02	−1.12	0.35	−1.01	1.02	−1.12	0.35	−1.01	−1.24	−1.24
valency	2.65	1.05	1.26	1.12	2.65	1.05	1.26	1.12	0.72	0.72
bond orders										
Tl(1)	0.00									
Se(1)	0.54	0.00								
Tl(2)	0.09	0.33	0.00							
Se(2)	0.50	−0.04	0.33	0.00						
Tl(3)	0.11	−0.01	0.09	0.50	0.00					
Se(3)	−0.01	−0.02	0.33	−0.04	0.54	0.00				
Tl(4)	0.09	0.33	0.09	0.00	0.09	0.33	0.00			
Se(4)	0.50	−0.04	0.00	−0.06	0.50	−0.04	0.33	0.00		
Se(5)	0.83	−0.04	0.00	−0.03	0.00	0.00	0.00	−0.03	0.00	
Se(6)	0.00	0.00	0.00	−0.03	0.83	−0.04	0.00	−0.03	0.00	0.00

$Tl_5Se_5^{3-}$ (C_1, Crystal Structure))

atom	Tl(1)	Se(1)	Tl(2)	Se(2)	Tl(3)	Se(3)	Tl(4)	Se(4)	Tl(5)	Se(5)
charge	0.41	−1.21	0.40	−1.03	0.39	−1.06	0.91	−1.06	0.39	−1.08
valency	1.30	1.08	1.31	1.15	1.54	1.23	3.14	1.24	1.42	0.95
bond orders										
Tl(1)	0.00									
Se(1)	0.39	0.00								
Tl(2)	0.10	0.38	0.00							
Se(2)	0.29	−0.02	0.29	0.00						
Tl(3)	0.11	0.41	0.11	0.00	0.00					
Se(3)	−0.01	−0.02	0.32	−0.04	0.29	0.00				
Tl(4)	0.15	−0.01	0.14	0.72	0.08	0.49	0.00			
Se(4)	0.29	−0.02	−0.01	−0.04	0.30	−0.05	0.52	0.00		
Tl(5)	−0.01	−0.02	−0.01	−0.01	0.27	0.30	0.29	0.29	0.00	
Se(5)	0.00	0.00	0.00	−0.03	−0.01	−0.05	0.77	−0.05	0.33	0.00

$Tl_5Se_5^{3-}$ (C_s, MP2 Optimized)

atom	Tl(1)	Se(1)	Tl(2)	Se(2)	Tl(3)	Se(3)	Tl(4)	Se(4)	Tl(5)	Se(5)
charge	0.44	−1.25	0.44	−1.06	0.38	−1.10	0.92	−1.10	0.41	−1.10
valency	1.21	1.02	1.21	1.09	1.33	1.18	3.02	1.18	1.27	0.93
bond orders										
Tl(1)	0.00									
Se(1)	0.37	0.00								
Tl(2)	0.09	0.37	0.00							
Se(2)	0.25	−0.02	0.25	0.00						
Tl(3)	0.10	0.35	0.10	0.00	0.00					
Se(3)	−0.01	−0.02	0.28	−0.04	0.29	0.00				
Tl(4)	0.14	−0.01	0.14	0.72	0.06	0.50	0.00			
Se(4)	0.28	−0.02	−0.01	−0.04	0.29	−0.06	0.50	0.00		
Tl(5)	−0.01	−0.01	−0.01	−0.01	0.16	0.28	0.25	0.27	0.00	
Se(5)	0.00	0.00	0.00	−0.03	−0.01	−0.05	0.72	−0.05	0.35	0.00

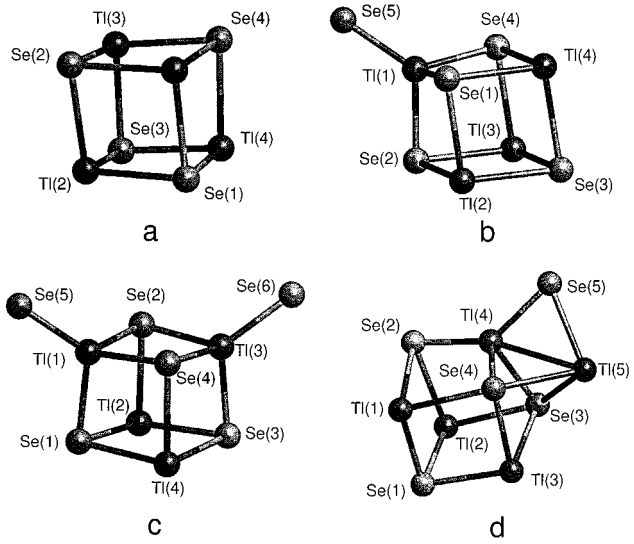

Figure 11. Calculated geometries at the MP2 level for the (a) $Tl_4Se_4^{4-}$, (b) $Tl_4Se_5^{4-}$, (c) $Tl_4Se_6^{4-}$, and (d) $Tl_5Se_5^{3-}$ anions.

optimization resulted in a transition state with three imaginary frequencies, one having e and two having t_1 symmetry. Optimizations following each of these five imaginary frequencies resulted in dissociation into four $TlSe^-$ anions. Taking electron correlation into account, MP2 optimization starting from the HF transition state structure resulted in a geometry having T_d symmetry (Figure 11a and Table 7), which is a true local minimum with all frequencies positive (Table 8).

The sum of ionic radii of Se^{2-} and Tl^+ (3.48 Å)[21] is clearly greater than the MP2 optimized Tl−Se distance of 3.134 Å (Table 7), indicating significant covalent bonding. The anion geometry is essentially a cube with bond angles very close to 90° and intrafacial torsion angles that are close to ±90° and 0° (Table 7).

(b) $Tl_4Se_5^{4-}$ and $Tl_4Se_6^{4-}$. Optimization using C_{3v} and C_{2v} symmetries, respectively, resulted in local minima at both the HF and MP2 levels. The optimized MP2 geometries are depicted in parts b and c of Figure 11, bond parameters are listed in Table 7, and the calculated fundamental frequencies are listed in Table 8.

(c) $Tl_5Se_5^{3-}$. Experimental and calculated MP2 optimized bond parameters are given in Table 2. As in the case of $Tl_4Se_4^{4-}$ (T_d), optimization at the HF level of theory starting with the experimental coordinates resulted in the breakage of several bonds. The MP2 optimization was carried out first in C_1 symmetry starting from the experimental geometry and led to a structure that was in excellent agreement with the crystal structure (Table 2). The optimized C_1 structure was very close to C_s symmetry so that equalization of the appropriate atomic coordinates converted it to C_s symmetry. By use of the C_s structure as a starting point, a further MP2 optimization was carried out resulting in essentially the same bonding parameters as the C_1 optimization (Table 2, Figure 11d).

2. Natural Bond Orbital (NBO) Analyses. NBO analysis is based on a method for optimally transforming a given wave function into a localized form corresponding to the one-center (LP = lone pair) and two-center (BP = bond pair) elements of the Lewis structure. In the first step, the original basis set is transformed into natural atomic orbitals (NAO). Natural charges on atoms, Mayer valencies, and overlap-corrected bond orders based on NAO electron populations provide estimates of the ionic and covalent components of the bonding and provide qualitative correlations with the bond distances. In the second step, a set of NBO's is formed from the NAO's. The set of high-occupancy NBO's, each doubly occupied, is said to represent the "natural Lewis structure" of the molecule. Delocalization effects appear as minor departures from this idealized localized picture.[35] The NBO analyses were carried out for the MP2 optimized structures using the MP2 electron density. Natural charges, Mayer NAO valencies (total atomic bond orders),[36] and overlap-weighted NAO bond orders are given in Table 6. The NAO populations and summaries of the NBO analyses for the calculated species are given in the Supporting Information.

Table 7. Calculated[a] Geometries (Bond Lengths (Å) and Bond Angles (deg)) for the $Tl_4Se_4^{4-}$(T_d), $Tl_4Se_5^{4-}$ (C_{3v}), and $Tl_4Se_6^{4-}$ (C_{2v}) Anions

	$Tl_4Se_4^{4-}$	$Tl_4Se_5^{4-}$	$Tl_4Se_6^{4-}$
Se(4)−Tl(1)	3.134	2.820	2.837
Se(4)−Tl(4)		3.083	3.056
Se(4)−Tl(3)		3.083	2.837
Tl(1)−Se(2)		2.820	2.837
Tl(1)−Se(1)		2.820	2.787
Tl(4)−Se(1)		3.083	3.067
Tl(4)−Se(3)		3.100	3.067
Se(2)−Tl(2)		3.083	3.056
Tl(1)−Se(5)		2.664	2.621
Tl(3)−Se(2)		3.083	2.837
Tl(3)−Se(3)		3.100	2.787
Se(1)−Tl(2)		3.083	3.067
Se(3)−Tl(2)		3.100	3.067
Tl(1)−Tl(4)	4.175	4.138	3.361
Tl(2)−Tl(4)		4.123	3.361
Tl(1)−Tl(3)		4.138	3.361
Se(1)−Tl(1)−Se(2)	96.1	96.0	97.3
Se(1)−Tl(1)−Se(4)		96.0	97.3
Se(1)−Tl(1)−Se(5)		120.9	119.7
Se(2)−Tl(1)−Se(4)		96.0	90.4
Se(2)−Tl(1)−Se(5)		120.9	122.6
Se(4)−Tl(1)−Se(5)		120.9	122.6
Tl(1)−Se(1)−Tl(2)	83.5	88.9	88.0
Tl(1)−Se(1)−Tl(4)		88.9	88.0
Tl(2)−Se(1)−Tl(4)		83.9	84.5
Se(1)−Tl(2)−Se(2)		85.6	87.1
Se(1)−Tl(2)−Se(3)		96.3	95.3
Se(2)−Tl(2)−Se(3)		96.3	87.1
Tl(1)−Se(2)−Tl(2)		88.9	87.4
Tl(1)−Se(2)−Tl(3)		88.9	89.2
Tl(2)−Se(2)−Tl(3)		83.9	87.4
Se(2)−Tl(3)−Se(3)		96.3	97.3
Se(2)−Tl(3)−Se(4)		85.6	90.4
Se(2)−Tl(3)−Se(6)			122.6
Se(3)−Tl(3)−Se(4)		96.3	97.3
Se(3)−Tl(3)−Se(6)			119.7
Se(4)−Tl(3)−Se(6)			122.6
Tl(2)−Se(3)−Tl(3)		83.4	88.0
Tl(2)−Se(3)−Tl(4)		83.4	84.5
Tl(3)−Se(3)−Tl(4)		83.4	88.0
Se(1)−Tl(4)−Se(3)		96.3	95.3
Se(1)−Tl(4)−Se(4)		85.6	87.1
Se(3)−Tl(4)−Se(4)		96.3	87.1
Tl(1)−Se(4)−Tl(3)		88.9	89.2
Tl(1)−Se(4)−Tl(4)		88.9	87.4
Tl(3)−Se(4)−Tl(4)		85.3	87.4

[a] Calculated geometries at the MP2 level.

(a) $Tl_4Se_4^{4-}$. Compared to pure ionic bonding ($4Tl^+ + 4Se^{2-}$), the Tl^I atoms gain electron density from the selenide ions, resulting in a charge of 0.33 instead of 1 for each Tl^I atom, leaving each Se atom with a charge of −1.33 instead of −2. This gain of electron density by Tl^I is attributable to partial covalent bonding between atoms that otherwise would be

(35) Glendening, E. D.; Reed, A. E.; Carpenter, J. E.; Weinhold, F. *NBO*, version 3.1; Gaussian, Inc.: Pittsburgh, PA, 1990.
(36) Mayer, I. *Chem. Phys. Lett.* **1983**, *97*, 270; *Theor. Chim. Acta* **1985**, *67*, 315; *Int. J. Quantum Chem.* **1986**, *29*, 73.

Table 8. Calculated[a] Fundamental Vibrational Frequencies (cm^{-1}) and Assignments for the $Tl_4Se_4^{4-}$, $Tl_4Se_5^{4-}$, $Tl_4Se_6^{4-}$, and $Tl_5Se_5^{3-}$ Anions

$Tl_4Se_4^{4-}$ (T_d)	$Tl_4Se_5^{4-}$ (C_{3v})	$Tl_4Se_6^{4-}$ (C_{2v})	$Tl_5Se_5^{3-}$ (C_s)
	27 (0), a_2	27 (0), a″	
30 (1), e	29 (2), a_1	31 (0), a′	
	38 (1), b_1	34 (0), a″	
	40 (0), b_2	37 (0), a′	
32 (0), e	42 (0), e	44 (0), b_2	44 (0), a″
37 (1), t_2	43 (0), a_2	51 (0), a_2	44 (0), a′
45 (0), t_2	48 (0), e	53 (0), b_2	45 (0), a′
45 (0), e	56 (0), e	54 (0), a_1	49 (0), a″
		58 (1), b_1	57 (0), a″
53 (0), a_1	65 (0), a_1	64 (0), a_2	64 (3), a′
	67 (1), a_1	71 (0), a_1	65 (0), a″
		76 (1), b_1	69 (0), a′
85 (74), t_2	90 (4), e	91 (8), b_2	72 (1), a′
95 (0), a_1	94 (1), e	101 (4), a_1	78 (1), a′
		103 (0), a_2	90 (2), a″
108 (24), t_2	112 (8), e	114 (24), b_1	101 (26), a′
	112 (40), a_1	116 (6), a_1	112 (35), a′
	121 (60), e	123 (75), b_2	114 (29), a′
	133 (1), a_1	135 (65), a_1	116 (1), a″
		135 (2), b_2	122 (40), a′
		137 (41), b_1	128 (56), a″
	159 (116), a_1	141 (2), a_1	141 (25), a′
		171 (137), b_2	154 (27), a′
		176 (62), a_1	185 (46), a′

[a] Uncorrected calculated values (MP2 level). When experimental frequencies are compared, these values should be multiplied by 0.94 to compensate for the systematic errors. Infrared intensities are given in parentheses in units of km mol^{-1}.

bonded by "pure" ionic bonds. Each Tl interacts with each adjacent Se to give a bond order of 0.32 along each cube edge and slightly repulsively (bond order, −0.02) with the opposite Se along the diagonal of the cube. In addition, each Tl interacts with the other three Tl atoms along the diagonals of the cube faces, providing a bond order of 0.09 and a total valency of 1.21 for Tl.

The anion has 40 valence electrons that are assigned by the NBO analysis to a natural Lewis structure with 12 bonding orbitals and 8 lone pairs, one on each atom. Of the 40 valence electrons, 38.4 electrons are described by this 8 LP−12 BP Lewis structure and 1.6 electrons are of a non-Lewis type.

(b) $Tl_4Se_5^{4-}$. The unique thallium atom, Tl(1), has more positive charge (1.03) and the highest valency (2.58) among the four Tl atoms, thus confirming the assignment of a formal oxidation state of +3 to Tl(1). The high charge of Se(5) (−1.30) and high Tl(1)−Se(5) bond order (0.79) indicate multiple bonding, resulting in a bond length (2.664 Å) that is significantly shorter than other Tl−Se bonds in this anion. The tendency of the Tl^{III} atom to act as a Lewis acid is further indicated by the lower negative charges (−1.14) on the adjacent Se(1), Se(2), and Se(4) atoms within the cube and by their high bond orders (0.52) with Tl(1), resulting in three short Tl^{III}−Se distances of 2.820 Å. Although the Se(3) atom is bonded to three Tl^{I} atoms and the exocyclic Se(5) atom is bonded to a single Tl^{III} atom, both selenium atoms have the same natural charges (−1.30), which gives Se(3) a higher valency (0.91) than Se(5) (0.67), but lower Tl−Se bond order (0.33) and the longest bonds (3.083−3.100 Å) when compared with those of Se(5) bonded to the unique Tl^{III} atom (0.79 and 2.664 Å, respectively) or with selenium bonded to the unique Tl^{III} atom and to two Tl^{I} atoms [Se(1), Se(2) and Se(4), 0.52 and 2.820 Å, respectively]. Thus, the lower bond orders and smaller charges associated with Se(3) bonded to Tl^{I} are corroborated by displaying the longest Tl^{I}−Se bonds with intermediate values for seleniums bonded to both Tl^{I} and Tl^{III}, and the highest bond order and selenium charge for the short exocyclic $Tl(4)^{III}$−Se(5) bond.

By default, an NBO analysis for this 46 valence electron anion assigns 10 lone pairs, one to each atom except for the Tl^{III} atom (Tl(1)), and a second lone pair to both Se(2) (or the equivalent adjacent Se(1), Se(2), or Se(4) atoms) and the exocyclic Se(5) atom. The cube framework comprises 11 bonding orbitals with 2 bonding orbitals assigned between Tl(1) and Se(5) for a total of 13 bonding electron pairs for the natural Lewis structure. The absence of bonding between Tl(1) and Se(2) in this analysis arises because there are already four bonds (an octet) to Tl(1). The "missing" bond is compensated for by a second lone pair on Se(2), which can be viewed as forming a donor−acceptor bond to Tl(1). Thus, 43.1 electrons are described by this 10 LP−13 BP Lewis structure and 2.9 electrons are of the non-Lewis type. This is one of three possible Lewis resonance structures for the C_{3v} symmetric anion. In an attempt to retain the C_{3v} symmetry for the NBO bonding by forming a single bond between Tl(1) and Se(2) from the second lone pair on Se(2), a 9 LP−14 BP Lewis structure resulted. This alternative structure describes 42.9 electrons by the Lewis structure, leaving 3.1 electrons as a non-Lewis type, and is only slightly inferior to the 10 LP-13 BP structure.

(c) $Tl_4Se_6^{4-}$. Two Tl atoms display high charges (1.02) and high valencies (2.65), namely, atoms Tl(1) and Tl(3), in accord with their formal oxidation states of +3. Both Se(5) and Se(6), which are terminally bonded to these Tl^{III} atoms, have slightly higher charges (−1.24) than Se(5) in $Tl_4Se_5^{4-}$ (−1.30); however, their higher valencies (0.72) compensate, resulting in slightly shorter terminal Tl^{III}−Se bonds (2.621 Å) than in $Tl_4Se_5^{4-}$ (2.668 Å). This indicates that the three lone pairs on the terminal Se atom are involved to a significant extent in bonding. The two Tl^{III} centers are more acidic, resulting in shorter intrafacial Tl^{III}−Se bonds (2.837 Å) than for the Tl^{I}−Se bonds in the opposite face (3.067 Å) and in $Tl_4Se_4^{4-}$ (3.134 Å). As in the case of $Tl_4Se_5^{4-}$, similar trends among Tl^{III}−Se (2.787 Å) and Tl^{I}−Se (3.134 Å) bond lengths are observed within the [Tl^{III}-SeTl^{I}Se] planes.

The $Tl_4Se_6^{4-}$ anion has 52 valence electrons. As a default, the NBO program assigns 12 lone pairs as follows: none to Tl(1) and Tl(3), three to Se(5) and Se(6), and one each to the remaining Tl^{I} and Se atoms. The remaining 14 electron pairs are assigned to single bonds between atoms to complete the natural Lewis structure. A total of 49.0 electrons are described by this 12 LP−14 BP Lewis structure, and 3.0 electrons are of a non-Lewis type. To account for the short Tl(1)−Se(5) and Tl(3)−Se(6) bond distances, the lone pairs on Se(5) and Se(6) can be regarded as forming donor−acceptor bonds to Tl(1) and Tl(3), resulting in multiple bonding. The rather high non-Lewis type electron count suggests that other resonance structure(s) should be considered. An alternative 10 LP−16 BP Lewis structure having double bonds between Tl^{III} and the terminal Se describes only 46.3 electrons, leaving 5.7 non-Lewis type electrons, thus providing no improvement over the default 12 LP−14 BP structure.

(d) $Tl_5Se_5^{3-}$. The calculated geometries at the MP2 level for both the experimental C_1 and optimized C_s symmetries are in excellent agreement with the X-ray crystal structure. Generally, the calculated bond lengths are somewhat longer (ca 0.1 Å) than the experimental ones. The angles within the distorted cube framework and to the capping thallium atom and bridge exo-selenium atom are also in good agreement with experimental results (Table 7).

(i) Experimental C_1 Geometry. The Tl(4) atom has a high charge (0.91) and a high total bond order (3.14). The latter is over three pure covalent bonds in addition to ionic interactions.

This assigns Tl(4) to a Tl^{III} atom, which is bonded to, as can be seen from the bond orders, Se(5) (0.77), Se(3) (0.49), Se(4) (0.52), and Se(2) (0.72). It is interesting to note that although Tl(4) and Tl(5) are both positive, with natural charges of 0.91 and 0.39, respectively, there is a significant positive bond order between Tl(4) and Tl(5) (0.29) so that Tl(4) has distorted trigonal bipyramidal coordination. The Tl(4)−Tl(5) bonding possibly arises as a result of the short Tl(4)−Tl(5) distance of 3.204(3) Å observed in the X-ray structure and contrasts with the other experimental Tl−Tl distances, i.e., Tl(1)−Tl(2) (4.007(2) Å), Tl(1)−Tl(3) (3.940(3) Å), Tl(1)−Tl(4) (3.780(3) Å), Tl(2)−Tl(3) (3.940(2) Å), Tl(2)−Tl(4) (3.746(3) Å), Tl(3)−Tl(4) (4.037(2) Å), and Tl(3)−Tl(5) (3.637(3) Å). As can be seen from the bond orders and experimental bond lengths (Table 2), the Tl(5) atom is essentially equivalently bonded to Se(3) (0.30), Se(4) (0.29), and Se(5) (0.33). In addition to Tl(4)−Tl(5) bonding, the experimental Tl(3)−Tl(5) distance is rather short (3.637(3) Å), giving a nearly equivalent bond order (0.27) with natural charges of 0.39 on both Tl(3) and Tl(5). The metal−metal interactions are reminiscent of those in the $Tl_2Ch_2^{2-}$,[2] $M_2Ch_3^{2-}$,[17] and $TlMTe_3^{3-}$ [17] (M = Sn, Pb; Ch = Se, Te) anions in which similar short Tl−Tl, M−M, and M−Tl distances were observed. The geometries and distances were reproduced by theoretical calculations, which also gave significant Mayer bond orders for these interactions.

The default NBO analysis for the experimental (C_1) symmetry of $Tl_5Se_5^{3-}$ assigns 12 lone pairs of this 48 valence electron system, one to each atom plus one extra pair on both Tl(5) and Se(5). The lone pair on Tl(4) has a low occupancy (0.41), and the occupancy for the second lone pair on Tl(5) is even lower (0.21). This leaves 12 electron pairs for bonding, which is insufficient for single bonds between each atom pair. The NBO analysis adds two three-center bonds to compensate. Only 42.1 electrons are described by the natural Lewis structure and 5.9 electrons are of a non-Lewis type. The default 12 LP−12 BP Lewis structure should be viewed with caution because the program indicates that the experimental anion conformation may be an excited state (i.e., not a local minimum energy ground state but a transition state).

An alternative bonding scheme assigning one lone pair each to Se(1), Se(2), Tl(1), Tl(2), Tl(3), and Tl(5) and two to Se(5), for a total of 8 lone pairs, leaves 16 electron pairs for bonding and is in accord with the single-bond description represented by Figure 11 in which each edge is a two center−two electron bond. This 8 LP−16 BP Lewis structure provides a more consistent explanation of the bonding, describing 43.6 valence electrons and leaving 4.4 electrons as non-Lewis types.

(ii) MP2 Optimized C_s Geometry. The most notable difference is that the atoms now have larger natural charges; that is, the bonding has slightly more ionic character, which is reflected in lower NAO valencies and bond orders than in the experimental conformation. The bond between Tl(3) and Tl(5) is now weaker with a bond order of 0.16 and natural charges of 0.38 and 0.41, respectively, resulting in a significantly longer bond distance (3.995 Å). Although the Tl(4)−Tl(5) distance (3.361 Å) is slightly longer than in the experimental geometry, the bonding interaction is still significant, with a somewhat lower bond order (0.25) and higher natural charges (0.91 and 0.41, respectively).

The default NBO Lewis structure assigns 13 lone pairs, one to each atom other than Se(2), Se(3), and Se(5), which are each assigned two electron lone pairs. The lone pair on Tl(4) has a low occupancy (0.31). This leaves only 11 electron pairs for bonding. The NBO analysis adds two three-center bonds to compensate. Only 43.4 electrons are described by this 13 LP−11 BP natural Lewis structure so that 4.6 electrons are of a non-Lewis type.

Table 9. MP2−Optimized Energies of the Thallium Selenide Anions, Polyselenides, Se_8, and Tl^+

species	energy[a] MP2	ZPE
Se_8	−74.248 356 9	0.006 624
Se_n^{2-}, $n = 1$	−9.135 738 5	0.000 000
$n = 2$	−18.469 005 1	0.000 490
$n = 3$	−27.794 992 3	0.001 286
$n = 4$	−37.107 738 1	0.002 111
$n = 5$	−46.413 506 5	0.002 931
$n = 6$	−55.713 525 2	0.003 767
Tl^+	−1.730 112 5	0.000 000
$Tl_4Se_4^{4-}$	−44.766 594 2	0.002 568
$Tl_4Se_5^{4-}$	−54.132 809 9	0.003 804
$Tl_4Se_6^{4-}$	−63.486 856 2	0.004 905
$Tl_5Se_5^{4-}$	−56.389 150 7	0.004 501
$TlSe_3^{3-}$	−29.661 889 9	0.001 541
$Tl_2Se_2^{2-}$	−22.534 758 1	0.001 246

[a] Electron and zero-point energies (ZPE) in au (1 au = 627.5 kcal mol^{-1}).

The same alternative 8 LP−16 BP Lewis structure results, as was obtained for the experimental C_1 geometry. The ability of two quite different Lewis structures to describe the bonding in $Tl_5Se_5^{3-}$ confirms the highly delocalized covalent bonding in this anion, as already discussed above using NAO bond orders and Mayer NAO valencies.

3. Summary. Ab initio molecular orbital calculations for molecules containing several heavy element atoms are possible when using effective core pseudopotential (ECP) basis sets. In the case of thallium, relativistic effects must be taken into account. Inclusion of electron correlation corrections, at least at the MP2 level of theory when optimizing structures, is essential in producing reliable results for structure and energy. Polarization functions must be added to the relativistic ECP basis set, especially for selenium, to reproduce the experimental geometrical parameters.

Natural bond orbital analyses provide a systematic means to localize the total molecular electron density into bonding electron pairs between atoms and into lone pairs on atoms. However, if the bonding is significantly delocalized, as for example in $Tl_4Se_5^{4-}$ and $Tl_4Se_6^{4-}$, default NBO analyses fail to produce consistent natural Lewis structures, leaving a shortage of electrons in the Lewis bonding scheme. In these cases, alternative Lewis structures must be analyzed in order to provide a better understanding of the localized bonding.

Interconversions among the Thallium Selenide Anions. The $^{205,203}Tl$ NMR spectra of the KTlSe and KTl^{77}Se extracts recorded at −40 °C reveal that the $Tl_4Se_5^{4-}$ and $Tl_4Se_6^{4-}$ anions are in equilibrium with each other (see NMR Study). The NMR study also revealed the coexistence of the known $TlSe_3^{3-}$, $Tl_2Se_2^{2-}$, and Se^{2-} anions. To formulate likely pathways to the thallium selenide, diselenide, and polyselenide anions observed in our solution NMR studies and single crystal X-ray structure determinations and to more fully understand the interconversions among these anions, the MP2 energies corrected with zero-point energies (ZPE) were used to estimate the gas-phase reaction enthalpies. The energies of the fully MP2-optimized geometries that were used for each species in the following discussion are collected in Table 9.

It was previously proposed[8] that the butterfly-shaped $Tl_2Se_2^{2-}$ anion is derived from the trigonal planar $TlSe_3^{3-}$ anion by means of a redox disproportionation (eq 1), and that, in part, the reaction accounts for the occurrence of the Se_2^{2-} anion in these

$$2TlSe_3^{3-} \rightarrow Tl_2Se_2^{2-} + 2Se_2^{2-}; \quad \Delta E = -94.0 \text{ kcal mol}^{-1} \quad (1)$$

solutions. The gas-phase reaction is shown to be exothermic, favoring the formation of the $Tl_2Se_2^{2-}$ and Se_2^{2-} anions as previously postulated. The presence of Se_2^{2-} has also been attributed to eqs 2 and 3. The enthalpies favor the formation of

$$Se_{n-1}^{2-} + {}^1/_8Se_8 \rightarrow Se_n^{2-} \quad (2)$$

$$\Delta E = -33.0 \text{ kcal mol}^{-1} (n = 2)$$
$$= -28.2 (n = 3)$$
$$= -19.9 (n = 4)$$
$$= -15.5 (n = 5)$$
$$= -11.9 (n = 4)$$

$$Se_{2n-1}^{2-} + Se^{2-} \rightarrow 2\,Se_n^{2-} \quad (3)$$

$$\Delta E = -4.8 \text{ kcal mol}^{-1} (n = 2)$$
$$= -25.8 \text{ kcal mol}^{-1} (n = 3)$$

the longer polyselenides, while shorter chain polyselenides are slightly more stable than longer chain ones.

Several plausible routes to the formation of the cubanoid anions observed in this study likely involve the $TlSe_3^{3-}$ and $Tl_2Se_2^{2-}$ anions, which are present in high concentrations in the solutions that have been studied. A dimerization process in which two $Tl_2Se_2^{2-}$ anions interact to form the intermediate cubanoid $Tl_4Se_4^{4-}$ anion (eq 4) is clearly unlikely on energetic

$$2Tl_2Se_2^{2-} \rightarrow Tl_4Se_4^{4-}; \quad \Delta E = 190.1 \text{ kcal mol}^{-1} \quad (4)$$

grounds. The high concentrations of $TlSe_3^{3-}$ that are present in these solutions suggest the mildly endothermic alternative, eq 5, which results from the combination of (2)(eq 1) + eq 4. This

$$4TlSe_3^{3-} \rightarrow Tl_4Se_4^{4-} + 4Se_2^{2-}; \quad \Delta E = 2.1 \text{ kcal mol}^{-1} \quad (5)$$

almost thermally neutral reaction would allow for small, but significant, equilibrium amounts of the anion intermediate, $Tl_4Se_4^{4-}$, and also would account for our failure to observe this anion by NMR spectroscopy in the course of the present study. The Se^{2-} anion was observed in the ^{77}Se NMR spectra in both NH_3 (−424 ppm, −70 °C; −439 ppm, −20 °C) and en (−433 ppm, 30 °C; −427 ppm, 0 °C) solutions of these systems, and the Se_5^{2-} anion was isolated as the crystalline (2,2,2-crypt-K^+)$_2$-Se_5^{2-} salt from an extract of KTlSe (see Experimental Section). The di- and polyselenide anions present in the solution presumably oxidatively add stepwise to the Tl^I centers of $Tl_4Se_4^{4-}$ to give the $Tl_4Se_5^{4-}$ (eq 6) and $Tl_4Se_6^{4-}$ (eq 7) anions, with both oxidation steps being energetically favored. This scheme alone

$$Tl_4Se_4^{4-} + Se_n^{2-} \rightarrow Tl_4Se_5^{4-} + Se_{n-1}^{2-}$$

$$\Delta E = -20.2 \text{ kcal mol}^{-1} (n = 2) \quad (6)$$
$$= -25.0 (n = 3)$$
$$= -33.3 (n = 4)$$
$$= -37.7 (n = 5)$$
$$= -41.3 (n = 6)$$

$$Tl_4Se_5^{4-} + Se_n^{2-} \rightarrow Tl_4Se_6^{4-} + Se_{n-1}^{2-}$$

$$\Delta E = -12.6 \text{ kcal mol}^{-1} (n = 2) \quad (7)$$
$$= -17.3 (n = 3)$$
$$= -25.7 (n = 4)$$
$$= -30.0 (n = 5)$$
$$= -33.6 (n = 6)$$
$$= -41.3 (n = 6)$$

does not, however, account for the formation of the $Tl_5Se_5^{3-}$ anion. Another route to the $Tl_4Se_5^{4-}$ and $Tl_4Se_6^{4-}$ anions that would also account for the $Tl_5Se_5^{3-}$ anion involves condensation reactions between $TlSe_3^{3-}$ and $Tl_2Se_2^{2-}$ (eqs 8 and 9). However,

$$2TlSe_3^{3-} + Tl_2Se_2^{2-} \rightarrow Tl_4Se_6^{4-} + 2Se^{2-}; \quad \Delta E = 63.3 \text{ kcal mol}^{-1} \quad (8)$$

$$TlSe_3^{3-} + 2Tl_2Se_2^{2-} \rightarrow Tl_5Se_5^{3-} + 2Se^{2-}; \quad \Delta E = 44.7 \text{ kcal mol}^{-1} \quad (9)$$

both reactions are significantly endothermic. A more likely route to the $Tl_5Se_5^{3-}$ anion is the highly exothermic reaction between $Tl_4Se_5^{4-}$, formed in eq 6, and the Tl^+ cation (eq 10), which, together with eq 11, would also account for our failure to observe a thallium NMR resonance for 2,2,2-crypt-Tl^+ or

$$Tl_4Se_5^{4-} + Tl^+ \rightarrow Tl_5Se_5^{3-}; \quad \Delta E = -329.8 \text{ kcal mol}^{-1} \quad (10)$$

$$2Tl^+ + 2Se^{2-} \rightarrow Tl_2Se_2^{2-}; \quad \Delta E = -503.1 \text{ kcal mol}^{-1} \quad (11)$$

for solvated Tl^+ cation in these systems.

Conclusion

The novel cubanoid $Tl_4Se_5^{4-}$ and $Tl_4Se_6^{4-}$ anions have been unambiguously characterized in solution by variable temperature ^{205}Tl, ^{203}Tl, and ^{77}Se NMR spectroscopy at their natural abundance levels and at 94.4% ^{77}Se-enrichment levels, and their structures were confirmed by full simulations and complete assignments of their isotopomeric ^{203}Tl and ^{205}Tl subspectra. The $Tl_5Se_5^{3-}$ anion was isolated as crystalline (2,2,2-crypt-K^+)$_3$-$Tl_5Se_5^{3-}$ and structurally characterized by X-ray crystallography. The structures of all three anions are based on a cube-shaped Tl_4Se_4 cage (T_d point symmetry) and contain exocyclic selenium bonded to a Tl^{III} center. The crystal structure of the $Tl_5Se_5^{3-}$ anion shows that it is formally derived from the $Tl_4Se_5^{4-}$ anion by adducting a Tl^+ cation to the exo-selenium and two seleniums within the cube framework. The geometries of all three anions have been shown to be energy-minimized structures, which can be described as electron-precise cages. The calculated gas-phase enthalpies support their derivation from the $TlSe_3^{3-}$, $Tl_2Se_2^{2-}$, Se_2^{2-}, and/or polyselenide anions that are also present in the solution extracts. The presently unknown $Tl_4Se_4^{4-}$ anion is shown to be a plausible intermediate in the formation of the $Tl_4Se_5^{4-}$ anion by oxidation of $Tl_4Se_4^{4-}$ with Se_2^{2-} or polyselenides and that, in turn, $Tl_4Se_5^{4-}$ can be readily oxidized in like manner to $Tl_4Se_6^{4-}$. The formation of $Tl_5Se_5^{3-}$ from Tl^+ and $Tl_4Se_5^{4-}$ is shown to be highly favorable.

Experimental Section

Apparatus and Materials. All compounds employed are air-sensitive. Consequently, all manipulations were performed under rigorously anhydrous conditions and in the absence of oxygen on a

glass vacuum line and in a two-station nitrogen-atmosphere drybox as previously described in ref 2.

Potassium metal (BDH Chemicals, >99%) was cleaned as previously described,[20] and freshly cut samples were handled in a drybox. Thallium rods (Alfa Inorganics, 99%), selenium shot (Alfa Inorganics, 99.9%), 94.4% ^{77}Se-enriched selenium (Technabsexport, Moscow, Russia), and 2,2,2-crypt (1,10-diaza-4,7,13,16,21,24-hexaoxabicyclo[8.8.8]hexacosane; Merck, 99%) were dried in the evacuated port of the drybox for a minimum of 45 min followed by exposure to the atmosphere of the drybox for at least 2 days prior to use. The oxide layer on the thallium rod was shaved off with a scalpel inside the drybox prior to use.

All solvents were thoroughly dried, transferred by vacuum distillation, and stored in round-bottom flasks equipped with glass/Teflon stopcocks (J. Young). Ethylenediamine (Fisher Scientific Co., 99%) and tetrahydrofuran (Aldrich, 99.9%) were initially dried over CaH_2 powder (BDH Chemicals, 99.5%) and sodium pieces (BDH Chemicals, 99.8%), respectively, for several weeks and then vacuum-distilled onto and stored over fresh CaH_2 powder and sodium, respectively, for at least an additional week prior to use. Anhydrous ammonia (Matheson, 99.99%) was condensed from a gas cylinder at −78 °C into a previously dried tube containing freshly cut sodium metal and stored at −78 °C for at least 1 week prior to use. Dimethylformamide (BDH Chemicals, 99%) was dried over 3 Å molecular sieves (Fisher Scientific), which were activated by heating under dynamic vacuum at ca. 250 °C overnight.

Preparation of KTlSe and KTl^{77}Se. The KTlSe alloy was prepared as previously described.[2] The 94.4% ^{77}Se-enriched KTlSe alloy (hereafter referred to as KTl^{77}Se) was prepared in two steps involving the fusion of KTl in a Pyrex tube followed by fusion with enriched ^{77}Se in a quartz vessel. The binary KTl phase was prepared by fusion of potassium (0.3157 g, 8.075 mmol) with the appropriate amount of thallium (1.6352 g, 8.001 mmol). The following amounts were used. KTlSe: K, 1.1424 g, 29.22 mmol; Tl, 5.976 g, 29.24 mmol; Se, 2.297 g, 29.04 mmol. KTl^{77}Se: KTl, 0.0803 g, 0.330 mmol; ^{77}Se, 0.0261 g, 0.331 mmol). The resulting alloys were ground into fine powders.

Preparation of the $Tl_4Se_5^{4-}$, $Tl_4{}^{77}Se_5^{4-}$, $Tl_4Se_6^{4-}$, $Tl_4{}^{77}Se_6^{4-}$, and $Tl_3Se_x^{y-}$ Solutions for NMR Spectroscopy. The anions were prepared by extracting KTlSe and KTl^{77}Se in en or liquid NH_3 in the presence of a 10−40 mol % excess of 2,2,2-crypt with respect to K^+. The resulting red solutions were isolated for NMR spectroscopy as previously described.[2] The following quantities of reagents were used to prepare the alloy extracts with values for the 94.4% ^{77}Se-enriched $Tl_4Se_x^{n-}$ anions given in brackets. Extraction in NH_3 (KTlSe, 0.1190 [0.1064] g, 0.3691 [0.3299] mmol; 2,2,2-crypt, 0.1894 [0.1474] g, 0.5031 [0.3915] mmol). Extraction in en (KTlSe, 0.1921 g, 0.5957 mmol; 2,2,2-crypt, 0.2183 g, 0.5798 mmol).

Multinuclear Magnetic Resonance Spectroscopy. The ^{203}Tl, ^{205}Tl, and ^{77}Se (−70 °C, NH_3) NMR spectra were recorded on a Bruker AC-200 (4.698 T) pulse spectrometer by inserting the 10 mm Bruker AC-300 broadbanded probe (13.968−121.497 MHz) into the AC-200 (4.698 T) cryomagnet. Other ^{77}Se NMR spectra (−20 °C, NH_3; 0 and 30 °C, en) were recorded on a Bruker AM-500 (11.744 T) pulse spectrometer. Spectra were routinely obtained without locking (field drift less than 0.1 Hz h^{-1}), using 10 mm probes broadbanded over the frequency ranges 9−81 (4.698 T) and 23−202 (11.744 T) MHz. The observed spectrometer frequencies were 38.168 (^{77}Se), 114.320 (^{203}Tl), and 115.447 (^{205}Tl) (4.698 T) and 95.383 (^{77}Se) (11.744 T) MHz. Free induction decays were typically accumulated in 16 or 32K memories. Spectral width settings of 25−100 kHz were employed, yielding data point resolutions of 3.05−6.10 Hz/data point and acquisition times of 0.328−0.164 s, respectively. A relaxation delay of 0.5 s was applied only for the ^{77}Se spectrum recorded on the AM-500. Typically, 10 000−100 000 transients were accumulated depending on the concentrations and sensitivities of the nuclides under study. Pulse-width settings corresponding to a bulk magnetization tip angle of ∼90° were 10.0 (^{205}Tl), 10.0 (^{77}Se, 11.744 T), and 20.0 (^{203}Tl) μs. Line broadening parameters used in the exponential multiplication of the free induction decays were 10−20 Hz for narrow lines and 100 Hz for broad lines. To enhance the resolution of some satellite peaks in the ^{205}Tl and ^{203}Tl NMR spectra and to determine the J couplings, the corresponding free induction decays were transformed with the use of Gaussian fits rather than with the conventional Lorentzian fits. For the Gaussian fits, Gaussian broadening factors between 0.1 and 0.5 and the negative of the line broadening parameters, which were used for Lorentzian fits, were employed in the multiplication. Variable-temperature spectra were recorded by using the variable-temperature controllers of the spectrometers, and temperatures (accurate to ±1.0 °C and stable to within ±0.10 °C) were checked by placing a copper constantan thermocouple into the sample region of the probe. Samples were allowed to equilibrate for at least 5 min while spinning before spectral accumulations were begun.

The ^{77}Se, ^{203}Tl, and ^{205}Tl chemical shifts were referenced externally to neat samples of $(CH_3)_2Se$ and 0.1 M aqueous $TlNO_3$ at 24 °C. The chemical shift convention used was a positive (negative) shift signifying a chemical shift to high (low) frequency of the reference sample.

Simulation of NMR Spectra. The ^{203}Tl and ^{205}Tl NMR spectra of the $Tl_4Se_5^{4-}$ and $Tl_4Se_6^{4-}$ anions were simulated on a 550 MHz Pentium III based computer using the computer program ISOTOPOMER.[26] The computational algorithm makes use of a direct expansion of a given cluster into all of its isotopomers. The starting data comprise the molecular point group symmetry, together with a list of symmetrically unrelated atoms and the symmetry elements on which they are situated. An internal table of symmetry elements for the group in question is then used to generate a complete list of atoms. The magnetic data are input as lists of independent reduced coupling constants and chemical shifts. The process begins with the calculation of the weights of all of the isotopomers belonging to a cluster using binomial coefficients and the isotopic abundances. Although the program has a threshold option allowing the rejection of those isotopomers whose weights are greater than or equal to a preselected weight, no thresholds were applied for the simulations described in this work. These selected isotopomers are further expanded into absolute isotopomers by taking all permutations of their isotopes among the sites within the molecule. The NMR Hamiltonian is then calculated for each of these absolute isotopomers and solved, and a spectrum is calculated. The resultant spectra are weighted according to their parent isotopomer's weight and added together to produce the total simulated NMR spectrum for the cluster. The program does not take into account isotopic effects on the chemical shift, which are assumed to be negligible for the present systems, but provides a full heteronuclear simulation that takes into account second-order effects. Spectra in the present study were not iterated.

Crystal Growth of (2,2,2-crypt-K^+)$_3Tl_5Se_5^{3-}$. In a previous paper,[2] we reported the formation of dark-red cubic crystals and red plates by extracting KTlSe in en in the presence of a molar excess of 2,2,2-crypt with respect to K^+, followed by vapor-phase diffusion of THF into the en solution. The dark-red cubes were shown to be (2,2,2-crypt-K^+)$_2Tl_2Se_2^{2-}$, while the red plates were found to consist of multiple crystals that failed to diffract. Extraction of KTlSe (0.1007 g, 0.3123 mmol) in DMF in the presence of a 20% molar excess of 2,2,2-crypt (0.1408 g, 0.3739 mmol) also gave rise to a red solution. Vapor diffusion of a slight excess of THF into the DMF extract resulted in the formation of numerous red plates of morphology similar to those previously observed in the en/THF mixtures. A red plate with the dimensions 0.40 × 0.09 × 0.02 mm^3 was mounted in a Lindemann glass capillary and used for the X-ray crystal structure determination. It should be noted that degradation of the crystals occurred when they were dried under dynamic vacuum for 2−3 min.

Collection and Reduction of X-ray Data. Crystal data were collected on a Stoe imaging plate diffractometer system equipped with a one-circle goniometer and a graphite monochromator. Molybdenum radiation (λ = 0.710 73 Å) was used. Integrated diffraction intensities were obtained at a crystal-to-detector distance of 70 mm, using oscillation scans with $-13 \le h \le 13$, $-19 \le k \le 19$, $-28 \le l \le 31$, and $9 \le 2\theta \le 50°$ and using 500 exposures (4.5 min per exposure) with $0 \le \varphi \le 200°$; the crystal oscillated 0.4° in $\Delta\varphi$. A total of 22 628 reflections were measured, and 13 465 remained after averaging of equivalent reflections. Corrections were made for Lorentz and polarization effects, and no absorption correction was applied.

Solution and Refinement of the Structures. All calculations were performed on a Silicon Graphics, Inc., model 4600PC workstation using

the SHELXTL-Plus package[37] for structure determination, refinement, and molecular graphics.

The XPREP program[37] was used to confirm the unit cell dimensions and the crystal lattice. The solution was obtained using conventional direct methods that located the general positions of the thallium, selenium, and potassium atoms, revealing the presence of a cubanoid-type anion, $Tl_5Se_5^{3-}$. The full-matrix least-squares refinement of the positions and isotropic thermal parameters of the assigned atoms located the general positions of the C, N, and O atoms of the (2,2,2-crypt-K^+) cations. The structure was then refined using anisotropic thermal parameters for all heavy atoms. The residual electron densities, in the final difference Fourier maps, were located around the anion but also in channels running parallel to the *a* axis, which are suspected to contain disordered solvent molecules (vide supra). The disorder, however, was too severe to allow the partial location of these molecules.

Calculations. The calculations were performed with the program Gaussian 98[38] at the ab initio Hartree−Fock (HF) and Møller−Plesset perturbation correction[39] for electron correlation to the second-order (MP2)[40−44] levels of theory. Stuttgart relativistic large core (RLC) effective core pseudopotential (ECP)[45,46] basis sets augmented with two d-type polarization functions by Huzinaga[47] were used for all calculated species. The geometries were fully optimized at both HF and MP2 levels using analytical gradient methods. The natural bond orbital (NBO) analysis method of Weinhold and co-workers[35,48−55] was used to obtain NBO natural Lewis structures, natural atomic charges, natural atomic orbital (NAO) bond orders,[56−58] and Mayer NAO valencies,[36] which were calculated using the program NBO, version 3.1,[35] as implemented in the Gaussian 98 program package.[38]

Acknowledgment. We thank the Natural Sciences and Engineering Research Council (NSERC) of Canada for support in the form of a research grant. We also thank NSERC and the Ontario Ministry of Education and Training for the award of graduate scholarships to J.C. We gratefully acknowledge Prof. Arndt Simon, Max-Planck-Institut, Stuttgart, Germany for making the Stoe imaging plate diffractometer system available and CSC−Tieteellinen laskenta Oy, Espoo, Finland for their generous contribution of computer time.

Supporting Information Available: Tables (S10, S11, and S12) reporting the MP2 valence natural atomic orbital populations (S10), the MP2 natural bond orbital analysis (S11), and the calculated bond parameters at the HF level (S12) for the $Tl_4Se_4^{4-}$, $Tl_4Se_5^{4-}$, $Tl_4Se_6^{4-}$, and $Tl_5Se_5^{3-}$ anions and an X-ray crystallographic file in CIF format for the structure determination of (2,2,2-crypt-K^+)$_3Tl_5Se_5^{3-}$. This material is available free of charge via the Internet at http://pubs.acs.org.

IC000779D

(37) Sheldrick, G. M. *SHELXTL-Plus*, release 4.21/V; Siemens Analytical X-ray Instruments Inc.: Madison, WI, 1993.
(38) Frisch, M. J.; Trucks, G. W.; Schlegel, H. B.; Scuseria, G. E.; Robb, M. A.; Cheeseman, J. R.; Zakrzewski, V. G.; Montgomery, J. A., Jr.; Stratmann, R. E.; Burant, J. C.; Dapprich, S.; Millam, J. M.; Daniels, A. D.; Kudin, K. N.; Strain, M. C.; Farkas, O.; Tomasi, J.; Barone, V.; Cossi, M.; Cammi, R.; Mennucci, B.; Pomelli, C.; Adamo, C.; Clifford, S.; Ochterski, J.; Petersson, G. A.; Ayala, P. Y.; Cui, Q.; Morokuma, K.; Malick, D. K.; Rabuck, A. D.; Raghavachari, K.; Foresman, J. B.; Cioslowski, J.; Ortiz, J. V.; Stefanov, B. B.; Liu, G.; Liashenko, A.; Piskorz, P.; Komaromi, I.; Gomperts, R.; Martin, R. L.; Fox, D. J.; Keith, T.; Al-Laham, M. A.; Peng, C. Y.; Nanayakkara, A.; Gonzalez, C.; Challacombe, M.; Gill, P. M. W.; Johnson, B. G.; Chen, W.; Wong, M. W.; Andres, J. L.; Head-Gordon, M.; Replogle, E. S.; Pople, J. A. *Gaussian 98*, revision A.7; Gaussian, Inc.: Pittsburgh, PA, 1998.
(39) Møller, C.; Plesset, M. S. *Phys. Rev.* **1934**, *46*, 618.
(40) Head-Gordon, M.; Pople, J. A.; Frisch, M. J. *Chem. Phys. Lett.* **1988**, *153*, 503.
(41) Frisch, M. J.; Head-Gordon, M.; Pople, J. A. *Chem. Phys. Lett.* **1990**, *166*, 275.
(42) Frisch, M. J.; Head-Gordon, M.; Pople, J. A. *Chem. Phys. Lett.* **1990**, *166*, 281.
(43) Head-Gordon, M.; Head-Gordon, T. *Chem. Phys. Lett.* **1994**, *220*, 122.
(44) Saebo, S.; Almlof, J. *Chem. Phys. Lett.* **1989**, *154*, 83.
(45) Igel-Mann, G.; Stoll, H.; Preuss, H. *Mol. Phys.* **1988**, *65*, 1321.
(46) Kuechle, W.; Dolg, M.; Stoll, H.; Preuss, H. *Mol. Phys.* **1991**, *74*, 1245.
(47) Huzinaga, S.; Andzelm, J.; Klobukowski, M.; Radzio-Andzelm, E.; Sakai, Y.; Tatewaki, H. *Gaussian Basis Sets for Molecular Calculations*; Physical Science Data 16; Elsevier: Amsterdam, 1984.
(48) Carpenter, J. E.; Weinhold, F. *J. Mol. Struct.: THEOCHEM* **1988**, *169*, 41.
(49) Carpenter, J. E. Ph.D. Thesis, University of Wisconsin, Madison, WI, 1987.
(50) Foster, J. P.; Weinhold, F. *J. Am. Chem. Soc.* **1980**, *102*, 7211.
(51) Reed, A. E.; Weinhold, F. *J. Chem. Phys.* **1983**, *78*, 4066.
(52) Reed, A. E.; Weinstock, R. B.; Weinhold, F. *J. Chem. Phys.* **1985**, *83*, 735.
(53) Reed, A. E.; Weinhold, F. *J. Chem. Phys.* **1985**, *83*, 1736.
(54) Reed, A. E.; Curtiss, L. A.; Wienhold, F. *Chem. Rev.* **1988**, *88*, 899.
(55) Weinhold, F.; Carpenter, J. E. *The Structure of Small Molecules and Ions*; Plenum: New York, 1988, p 227.
(56) Jensen, F. *Introduction to Computational Chemistry*; Wiley: New York, 1999; pp 217−234.
(57) Reed, A. E.; Schleyer, P. v. R. *Inorg. Chem.* **1988**, *27*, 3969.
(58) Reed, A. E.; Schleyer, P. v. R. *J. Am. Chem. Soc.* **1990**, *112*, 1434.